

Kernel-based Inference of Functions over Graphs

Vassilis N. Ioannidis^{*}, Meng Ma^{*}, Athanasios N. Nikolakopoulos^{*},
Georgios B. Giannakis^{*}, and Daniel Romero^{† *}

April 12, 2018

To be published as a chapter in ‘**Adaptive Learning Methods for Nonlinear System Modeling**’, Elsevier Publishing, Eds. D. Comminiello and J.C. Principe (2018)

Abstract

The study of networks has witnessed an explosive growth over the past decades with several ground-breaking methods introduced. A particularly interesting – and prevalent in several fields of study – problem is that of *inferring a function defined over the nodes of a network*. This work presents a versatile kernel-based framework for tackling this inference problem that naturally subsumes and generalizes the reconstruction approaches put forth recently by the signal processing on graphs community. Both the *static* and the *dynamic* settings are considered along with effective modeling approaches for addressing real-world problems. The herein analytical discussion is complemented by a set of numerical examples, which showcase the effectiveness of the presented techniques, as well as their merits related to state-of-the-art methods.

Index terms— Signal Processing on Graphs, Kernel-based learning, Graph function reconstruction, Dynamic graphs, Kernel Kalman filter

1 Introduction

Numerous applications arising in diverse disciplines involve *inference over networks* [1]. Modelling nodal attributes as signals that take values over the vertices of the underlying graph, allows the associated inference tasks to leverage node dependencies captured by the graph structure. In many real settings one often affords to work with only a limited number of node observations due to inherent restrictions particular to the inference task at hand. In social networks, for example, individuals may be reluctant to share personal information; in sensor networks the nodes may report observations sporadically in order to save energy;

^{**} ECE Dept. and the Digital Tech. Center, Univ. of Minnesota, Mpls, MN 55455, USA. E-mails: {ioann006,maxxx971,anikolak,georgios}@umn.edu, and [†] Dept. of Information and Communication Technology University of Agder, Grimstad, Norway E-mail: daniel.romero@uia.no

in brain networks acquiring node samples may involve invasive procedures (e.g. electrocorticography). In this context, a frequently encountered challenge that often emerges is that of *inferring the attributes for every node in the network given the attributes for a subset of nodes*. This is typically formulated as the task of reconstructing a function defined on the nodes [1–6], given information about some of its values.

Reconstruction of functions over graphs has been studied by the machine learning community, in the context of *semi-supervised learning* under the term of *transductive* regression and classification [6–8]. Existing approaches assume “smoothness” with respect to the graph – in the sense that neighboring vertices have similar values – and devise *nonparametric* methods [2, 3, 6, 9] targeting primarily the task of reconstructing binary-valued signals. Function estimation has also been investigated recently by the community of signal processing on graphs (SPoG) under the term *signal reconstruction* [10–17]. Most such approaches commonly adopt *parametric* estimation tools, and rely on *bandlimitedness*, by which the signal of interest is assumed to lie in the span of the B principal eigenvectors of the graph’s Laplacian (or adjacency) matrix.

This chapter cross-pollinates ideas arising from both communities, and presents a unifying framework for tackling signal reconstruction problems both in the traditional *time-invariant*, as well as in the more challenging *time-varying* setting. We begin by a comprehensive presentation of kernel-based learning for solving problems of signal reconstruction over graphs (Section 2). Data-driven techniques are then presented based on multi-kernel learning (MKL) that enables combining optimally the kernels in a given dictionary, and simultaneously estimating the graph function by solving a single optimization problem (Section 2.3). For the case where prior information is available, semi-parametric estimators are discussed that can incorporate seamlessly structured prior information into the signal estimators (Section 2.4). We then move to the problem of reconstructing time-evolving functions on dynamic graphs (Section 3). The kernel-based framework is now extended to accommodate the time-evolving setting building on the notion of *graph extension*, specific choices of which can lend themselves to a reduced complexity online solver (Section 3.1). Next, a more flexible model is introduced that captures multiple forms of time dynamics, and kernel-based learning is employed to derive an online solver, that effects online MKL by selecting the optimal combination of kernels on-the-fly (Section 3.2). Our analytical exposition, in both parts, is supplemented by a set of numerical tests based on both real and synthetic data that highlight the effectiveness of the methods, while providing examples of interesting realistic problems that they can address.

Notation: Scalars are denoted by lowercase characters, vectors by bold lowercase, matrices by bold uppercase; $(A)_{m,n}$ is the (m,n) -th entry of matrix \mathbf{A} ; superscripts T and \dagger respectively denote transpose and pseudo-inverse. If $\mathbf{A} := [\mathbf{a}_1, \dots, \mathbf{a}_N]$, then $\text{vec}\{\mathbf{A}\} := [\mathbf{a}_1^T, \dots, \mathbf{a}_N^T]^T := \mathbf{a}$. With $N \times N$ matrices $\{\mathbf{A}_t\}_{t=1}^T$ and $\{\mathbf{B}_t\}_{t=2}^T$ satisfying $\mathbf{A}_t = \mathbf{A}_t^T \forall t$, $\text{btridiag}\{\mathbf{A}_1, \dots, \mathbf{A}_T; \mathbf{B}_2, \dots, \mathbf{B}_T\}$ represents the symmetric block tridiagonal matrix. Symbols \odot , \otimes , and \oplus respectively denote element-wise (Hadamard) matrix product, Kronecker product,

and Kronecker sum, the latter being defined for $\mathbf{A} \in \mathbb{R}^{M \times M}$ and $\mathbf{B} \in \mathbb{R}^{N \times N}$ as $\mathbf{A} \oplus \mathbf{B} := \mathbf{A} \otimes \mathbf{I}_N + \mathbf{I}_M \otimes \mathbf{B}$. The n -th column of the identity matrix \mathbf{I}_N is represented by $\mathbf{i}_{N,n}$. If $\mathbf{A} \in \mathbb{R}^{N \times N}$ is positive definite and $\mathbf{x} \in \mathbb{R}^N$, then $\|\mathbf{x}\|_{\mathbf{A}}^2 := \mathbf{x}^T \mathbf{A}^{-1} \mathbf{x}$ and $\|\mathbf{x}\|_2 := \|\mathbf{x}\|_{\mathbf{I}_N}$. The cone of $N \times N$ positive definite matrices is denoted by \mathbb{S}_+^N . Finally, $\delta[\cdot]$ stands for the Kronecker delta, and \mathbb{E} for expectation.

2 Reconstruction of Functions over Graphs

Before giving the formal problem statement, it is instructive to start with the basic definitions that will be used throughout this chapter.

Definitions: A graph can be specified by a tuple $\mathcal{G} := (\mathcal{V}, \mathbf{A})$, where $\mathcal{V} := \{v_1, \dots, v_N\}$ is the vertex set, and \mathbf{A} is the $N \times N$ adjacency matrix, whose (n, n') -th entry, $A_{n,n'} \geq 0$, denotes the non-negative edge weight between vertices v_n and $v_{n'}$. For simplicity, it is assumed that the graph has no self-loops, i.e. $A_{n,n} = 0, \forall v_n \in \mathcal{V}$. This chapter focuses on *undirected* graphs, for which $A_{n',n} = A_{n,n'} \forall v_n, v_{n'} \in \mathcal{V}$. A graph is said to be *unweighted* if $A_{n,n'}$ is either 0 or 1. The edge set is defined as $\mathcal{E} := \{(v_n, v_{n'}) \in \mathcal{V} \times \mathcal{V} : A_{n,n'} \neq 0\}$. Two vertices v_n and $v_{n'}$ are *adjacent*, *connected*, or *neighbors* if $(v_n, v_{n'}) \in \mathcal{E}$. The *Laplacian* matrix is defined as $\mathbf{L} := \text{diag}\{\mathbf{A}\mathbf{1}\} - \mathbf{A}$, and is symmetric and positive semidefinite [1, Ch. 2]. A real-valued function (or signal) on a graph is a map $f : \mathcal{V} \rightarrow \mathbb{R}$. The value $f(v)$ represents an attribute or feature of $v \in \mathcal{V}$, such as age, political alignment, or annual income of a person in a social network. Signal f is thus represented by $\mathbf{f} := [f(v_1), \dots, f(v_N)]^T$.

Problem statement. Suppose that a collection of noisy samples (or observations) $\{y_s | y_s = f(v_{n_s}) + e_s\}_{s=1}^S$ is available, where e_s models noise and $\mathcal{S} := \{n_1, \dots, n_S\}$ contains the indices $1 \leq n_1 < \dots < n_S \leq N$ of the sampled vertices, with $S \leq N$. Given $\{(n_s, y_s)\}_{s=1}^S$, and assuming knowledge of \mathcal{G} , the goal is to estimate f . This will provide estimates of $f(v)$ both at observed and unobserved vertices. By defining $\mathbf{y} := [y_1, \dots, y_S]^T$, the observation model is summarized as

$$\mathbf{y} = \mathbf{S}\mathbf{f} + \mathbf{e} \tag{1}$$

where $\mathbf{e} := [e_1, \dots, e_S]^T$ and \mathbf{S} is a known $S \times N$ binary sampling matrix with entries $(s, n_s), s = 1, \dots, S$, set to one, and the rest set to zero.

2.1 Kernel Regression

Kernel methods constitute the “workhorse” of machine learning for nonlinear function estimation [18]. Their popularity can be attributed to their simplicity, flexibility, and good performance. Here, we present kernel regression as a unifying framework for graph signal reconstruction along with the so-called representer theorem.

Kernel regression seeks an estimate of f in a reproducing kernel Hilbert space

(RKHS) \mathcal{H} , which is the space of functions $f : \mathcal{V} \rightarrow \mathbb{R}$ defined as

$$\mathcal{H} := \left\{ f : f(v) = \sum_{n=1}^N \alpha_n \kappa(v, v_n), \alpha_n \in \mathbb{R} \right\} \quad (2)$$

where the *kernel map* $\kappa : \mathcal{V} \times \mathcal{V} \rightarrow \mathbb{R}$ is any function defining a symmetric and positive semidefinite $N \times N$ matrix with entries $[\mathbf{K}]_{n,n'} := \kappa(v_n, v_{n'})$ [19]. Intuitively, $\kappa(v, v')$ is a basis function in (2) measuring similarity between the values of f at v and v' . (For a more detailed treatment of RKHS, see e.g. [3]).

Note that for signals over graphs, the expansion in (2) is finite since \mathcal{V} is finite-dimensional. Thus, any $f \in \mathcal{H}$ can be expressed in compact form

$$\mathbf{f} = \mathbf{K}\boldsymbol{\alpha} \quad (3)$$

for some $N \times 1$ vector $\boldsymbol{\alpha} := [\alpha_1, \dots, \alpha_N]^T$.

Given two functions $f(v) := \sum_{n=1}^N \alpha_n \kappa(v, v_n)$ and $f'(v) := \sum_{n=1}^N \alpha'_n \kappa(v, v_n)$, their RKHS inner product is defined as¹

$$\langle f, f' \rangle_{\mathcal{H}} := \sum_{n=1}^N \sum_{n'=1}^N \alpha_n \alpha'_{n'} \kappa(v_n, v_{n'}) = \boldsymbol{\alpha}^T \mathbf{K} \boldsymbol{\alpha}' \quad (4)$$

where $\boldsymbol{\alpha}' := [\alpha'_1, \dots, \alpha'_N]^T$ and the reproducing property has been employed that suggests $\langle \kappa(\cdot, v_{n_0}), \kappa(\cdot, v_{n'_0}) \rangle_{\mathcal{H}} = \mathbf{i}_{n_0}^T \mathbf{K} \mathbf{i}_{n'_0} = \kappa(v_{n_0}, v_{n'_0})$. The RKHS norm is defined by

$$\|f\|_{\mathcal{H}}^2 := \langle f, f \rangle_{\mathcal{H}} = \boldsymbol{\alpha}^T \mathbf{K} \boldsymbol{\alpha} \quad (5)$$

and will be used as a regularizer to control overfitting and to cope with the under-determined reconstruction problem. As a special case, setting $\mathbf{K} = \mathbf{I}_N$ recovers the standard inner product $\langle f, f' \rangle_{\mathcal{H}} = \mathbf{f}^T \mathbf{f}'$, and the Euclidean norm $\|f\|_{\mathcal{H}}^2 = \|\mathbf{f}\|_2^2$. Note that when $\mathbf{K} \succ \mathbf{0}$, the set of functions of the form (3) coincides with \mathbb{R}^N .

Given $\{y_s\}_{s=1}^S$, RKHS-based function estimators are obtained by solving functional minimization problems formulated as (see also e.g. [18–20])

$$\hat{f} := \arg \min_{f \in \mathcal{H}} \mathcal{L}(\mathbf{y}, \bar{\mathbf{f}}) + \mu \Omega(\|f\|_{\mathcal{H}}) \quad (6)$$

where the loss \mathcal{L} measures how the estimated function f at the observed vertices $\{v_{n_s}\}_{s=1}^S$, collected in $\bar{\mathbf{f}} := [f(v_{n_1}), \dots, f(v_{n_S})]^T = \mathbf{S}\mathbf{f}$, deviates from the data \mathbf{y} . The so-called *square loss* $\mathcal{L}(\mathbf{y}, \bar{\mathbf{f}}) := (1/S) \sum_{s=1}^S [y_s - f(v_{n_s})]^2$ constitutes a popular choice for \mathcal{L} . The increasing function Ω is used to promote smoothness with typical choices including $\Omega(\zeta) = |\zeta|$ and $\Omega(\zeta) = \zeta^2$. The regularization

¹While f denotes a *function*, $f(v)$ represents the *scalar* resulting from evaluating f at vertex v .

parameter $\mu > 0$ controls overfitting. Substituting (3) and (5) into (6) shows that $\hat{\mathbf{f}}$ can be found as

$$\hat{\boldsymbol{\alpha}} := \arg \min_{\boldsymbol{\alpha} \in \mathbb{R}^N} \mathcal{L}(\mathbf{y}, \mathbf{S}\mathbf{K}\boldsymbol{\alpha}) + \mu\Omega((\boldsymbol{\alpha}^T \mathbf{K}\boldsymbol{\alpha})^{1/2}) \quad (7a)$$

$$\hat{\mathbf{f}} = \mathbf{K}\hat{\boldsymbol{\alpha}}. \quad (7b)$$

An alternative form of (5) that will be frequently used in the sequel results upon noting that

$$\boldsymbol{\alpha}^T \mathbf{K}\boldsymbol{\alpha} = \boldsymbol{\alpha}^T \mathbf{K}\mathbf{K}^\dagger \mathbf{K}\boldsymbol{\alpha} = \mathbf{f}^T \mathbf{K}^\dagger \mathbf{f}. \quad (8)$$

Thus, one can rewrite (6) as

$$\hat{\mathbf{f}} := \arg \min_{\mathbf{f} \in \mathcal{R}\{\mathbf{K}\}} \mathcal{L}(\mathbf{y}, \mathbf{S}\mathbf{f}) + \mu\Omega((\mathbf{f}^T \mathbf{K}^\dagger \mathbf{f})^{1/2}). \quad (9)$$

Although graph signals can be reconstructed from (7), such an approach involves optimizing over N variables. Thankfully, the solution can be obtained by solving an optimization problem in S variables (where typically $S \ll N$), by invoking the so-called representer theorem [19, 21].

The representer theorem plays an instrumental role in the traditional infinite-dimensional setting where (6) cannot be solved directly; however, even when \mathcal{H} comprises graph signals, it can still be beneficial to reduce the dimension of the optimization in (7). The theorem essentially asserts that the solution to the functional minimization in (6) can be expressed as

$$\hat{f}(v) = \sum_{s=1}^S \bar{\alpha}_s \kappa(v, v_{n_s}) \quad (10)$$

for some $\bar{\alpha}_s \in \mathbb{R}$, $s = 1, \dots, S$.

The representer theorem shows the form of \hat{f} , but does not provide the optimal $\{\bar{\alpha}_s\}_{s=1}^S$, which are found after substituting (10) into (6), and solving the resulting optimization problem with respect to these coefficients. To this end, let $\bar{\boldsymbol{\alpha}} := [\bar{\alpha}_1, \dots, \bar{\alpha}_S]^T$, and write $\boldsymbol{\alpha} = \mathbf{S}^T \bar{\boldsymbol{\alpha}}$ to deduce that

$$\hat{\mathbf{f}} = \mathbf{K}\boldsymbol{\alpha} = \mathbf{K}\mathbf{S}^T \bar{\boldsymbol{\alpha}}. \quad (11)$$

With $\bar{\mathbf{K}} := \mathbf{S}\mathbf{K}\mathbf{S}^T$ and using (7) and (11), the optimal $\bar{\boldsymbol{\alpha}}$ can be found as

$$\hat{\bar{\boldsymbol{\alpha}}} := \arg \min_{\bar{\boldsymbol{\alpha}} \in \mathbb{R}^S} \mathcal{L}(\mathbf{y}, \bar{\mathbf{K}}\bar{\boldsymbol{\alpha}}) + \mu\Omega((\bar{\boldsymbol{\alpha}}^T \bar{\mathbf{K}}\bar{\boldsymbol{\alpha}})^{1/2}). \quad (12)$$

Kernel ridge regression. For \mathcal{L} chosen as the square loss and $\Omega(\zeta) = \zeta^2$, the \hat{f} in (6) is referred to as the *kernel ridge regression* (RR) estimate [18]. If $\bar{\mathbf{K}}$ is full rank, this estimate is given by $\hat{\mathbf{f}}_{\text{RR}} = \mathbf{K}\mathbf{S}^T \hat{\bar{\boldsymbol{\alpha}}}$, where

$$\hat{\bar{\boldsymbol{\alpha}}} := \arg \min_{\bar{\boldsymbol{\alpha}} \in \mathbb{R}^S} \frac{1}{S} \|\mathbf{y} - \bar{\mathbf{K}}\bar{\boldsymbol{\alpha}}\|^2 + \mu \bar{\boldsymbol{\alpha}}^T \bar{\mathbf{K}}\bar{\boldsymbol{\alpha}} \quad (13a)$$

$$= (\bar{\mathbf{K}} + \mu S \mathbf{I}_S)^{-1} \mathbf{y}. \quad (13b)$$

Therefore, $\hat{\mathbf{f}}_{\text{RR}}$ can be expressed as

$$\hat{\mathbf{f}}_{\text{RR}} = \mathbf{K}\mathbf{S}^T(\bar{\mathbf{K}} + \mu S\mathbf{I}_S)^{-1}\mathbf{y}. \quad (14)$$

As we will see in the next section, (14) generalizes a number of existing signal reconstructors upon properly selecting \mathbf{K} .

2.2 Kernels on Graphs

When estimating functions on graphs, conventional kernels such as the Gaussian kernel cannot be adopted because the underlying set where graph signals are defined is not a metric space. Indeed, no vertex addition $v_n + v_{n'}$, scaling βv_n , or norm $\|v_n\|$ can be naturally defined on \mathcal{V} . An alternative is to embed \mathcal{V} into Euclidean space via a feature map $\phi : \mathcal{V} \rightarrow \mathbb{R}^D$, and invoke a conventional kernel afterwards. However, for a given graph it is generally unclear how to explicitly design ϕ or select D . This motivates the adoption of *kernels on graphs* [3].

A common approach to designing kernels on graphs is to apply a transformation function on the graph Laplacian [3]. The term *Laplacian kernel* comprises a wide family of kernels obtained by applying a certain function $r(\cdot)$ to the Laplacian matrix \mathbf{L} . Laplacian kernels are well motivated since they constitute the graph counterpart of the so-called *translation-invariant kernels* in Euclidean spaces [3]. This section reviews Laplacian kernels, provides beneficial insights in terms of interpolating signals, and highlights their versatility in capturing information about the *graph Fourier transform* of the estimated signal.

The reason why the graph Laplacian constitutes one of the prominent candidates for regularization on graphs, becomes clear upon recognizing that

$$\mathbf{f}^T \mathbf{L} \mathbf{f} = \frac{1}{2} \sum_{(n,n') \in \mathcal{E}} A_{n,n'} (f_n - f_{n'})^2, \quad (15)$$

where $A_{n,n'}$ denotes weight associated with edge (n, n') . The quadratic form of (15) becomes larger when function values vary a lot among connected vertices and therefore quantifies the *smoothness* of \mathbf{f} on \mathcal{G} .

Let $0 = \lambda_1 \leq \lambda_2 \leq \dots \leq \lambda_N$ denote the eigenvalues of the graph Laplacian matrix \mathbf{L} , and consider the eigendecomposition $\mathbf{L} = \mathbf{U}\mathbf{\Lambda}\mathbf{U}^T$, where $\mathbf{\Lambda} := \text{diag}\{\lambda_1, \dots, \lambda_N\}$. A Laplacian kernel matrix is defined by

$$\mathbf{K} := r^\dagger(\mathbf{L}) := \mathbf{U}r^\dagger(\mathbf{\Lambda})\mathbf{U}^T \quad (16)$$

where $r(\mathbf{\Lambda})$ is the result of applying a user-selected, scalar, non-negative map $r : \mathbb{R} \rightarrow \mathbb{R}_+$ to the diagonal entries of $\mathbf{\Lambda}$. The selection of map r generally depends on desirable properties that the target function is expected to have. Table 1 summarizes some well-known examples arising for specific choices of r .

At this point, it is prudent to offer interpretations and insights on the operation of Laplacian kernels. Towards this objective, note first that the regularizer

Kernel name	Function	Parameters
Diffusion [2]	$r(\lambda) = \exp\{\sigma^2\lambda/2\}$	σ^2
p -step random walk [3]	$r(\lambda) = (a - \lambda)^{-p}$	$a \geq 2, p \geq 0$
Regularized Laplacian [3, 22]	$r(\lambda) = 1 + \sigma^2\lambda$	σ^2
Bandlimited [23]	$r(\lambda) = \begin{cases} 1/\beta & \lambda \leq \lambda_{\max} \\ \beta & \text{otherwise} \end{cases}$	$\beta > 0, \lambda_{\max}$

Table 1: Common spectral weight functions.

from (9) is an increasing function of

$$\boldsymbol{\alpha}^T \mathbf{K} \boldsymbol{\alpha} = \boldsymbol{\alpha}^T \mathbf{K} \mathbf{K}^\dagger \mathbf{K} \boldsymbol{\alpha} = \mathbf{f}^T \mathbf{K}^\dagger \mathbf{f} = \mathbf{f}^T \mathbf{U} r(\boldsymbol{\Lambda}) \mathbf{U}^T \mathbf{f} = \check{\mathbf{f}}^T r(\boldsymbol{\Lambda}) \check{\mathbf{f}} = \sum_{n=1}^N r(\lambda_n) |\check{f}_n|^2 \quad (17)$$

where $\check{\mathbf{f}} := \mathbf{U}^T \mathbf{f} := [\check{f}_1, \dots, \check{f}_N]^T$ comprises the projections of \mathbf{f} onto the eigenspace of \mathbf{L} , and is referred to as the *graph Fourier transform* of \mathbf{f} in the SPoG parlance [4]. Consequently, $\{\check{f}_n\}_{n=1}^N$ are called *frequency components*. The so-called *bandlimited functions* in SPoG refer to those whose frequency components only exist inside some band B , that is, $\check{f}_n = 0, \forall n > B$.

By adopting the aforementioned SPoG notions, one can intuitively interpret the role of bandlimited kernels. Indeed, it follows from (17) that the regularizer strongly penalizes those \check{f}_n for which the corresponding $r(\lambda_n)$ is large, thus promoting a specific structure in this “frequency” domain. Specifically, one prefers $r(\lambda_n)$ to be large whenever $|\check{f}_n|^2$ is small and vice versa. The fact that $|\check{f}_n|^2$ is expected to decrease with n for smooth f , motivates the adoption of an increasing function r [3]. From (17) it is clear that $r(\lambda_n)$ determines how heavily \check{f}_n is penalized. Therefore, by setting $r(\lambda_n)$ to be small when $n \leq B$ and extremely large when $n > B$, one can expect the result to be a bandlimited signal.

Observe that Laplacian kernels can capture forms of prior information richer than bandlimitedness [11, 13, 16, 17] by selecting function r accordingly. For instance, using $r(\lambda) = \exp\{\sigma^2\lambda/2\}$ (diffusion kernel) accounts not only for smoothness of \mathbf{f} as in (15), but also for the prior that \mathbf{f} is generated by a process diffusing over the graph. Similarly, the use of $r(\lambda) = (\alpha - \lambda)^{-1}$ (1-step random walk) can accommodate cases where the signal captures a notion of network centrality².

So far, f has been assumed deterministic, which precludes accommodating certain forms of prior information that probabilistic models can capture, such

²Smola et al. [3], for example, discuss the connection between $r(\lambda) = (\alpha - \lambda)^{-1}$ and PageRank [24] whereby the sought-after signal is essentially defined as the limiting distribution of a simple underlying “*random surfing*” process. For more about random surfing processes, see also [25, 26].

as domain knowledge and historical data. Suppose without loss of generality that $\{f(v_n)\}_{n=1}^N$ are zero-mean random variables. The LMMSE estimator of \mathbf{f} given \mathbf{y} in (1) is the linear estimator $\hat{\mathbf{f}}_{\text{LMMSE}}$ minimizing $\mathbb{E}\|\mathbf{f} - \hat{\mathbf{f}}_{\text{LMMSE}}\|_2^2$, where the expectation is over all \mathbf{f} and noise realizations. With $\mathbf{C} := \mathbb{E}[\mathbf{f}\mathbf{f}^T]$, the LMMSE estimate is

$$\hat{\mathbf{f}}_{\text{LMMSE}} = \mathbf{C}\mathbf{S}^T[\mathbf{S}\mathbf{C}\mathbf{S}^T + \sigma_e^2\mathbf{I}_S]^{-1}\mathbf{y} \quad (18)$$

where $\sigma_e^2 := (1/S)\mathbb{E}[\|\mathbf{e}\|_2^2]$ denotes the noise variance. Comparing (18) with (14) and recalling that $\mathbf{K} := \mathbf{S}\mathbf{K}\mathbf{S}^T$, it follows that $\hat{\mathbf{f}}_{\text{LMMSE}} = \hat{\mathbf{f}}_{\text{RR}}$ if $\mu S = \sigma_e^2$ and $\mathbf{K} = \mathbf{C}$. In other words, the similarity measure $\kappa(v_n, v_{n'})$ embodied in such a kernel map is just the covariance $\text{cov}[f(v_n), f(v_{n'})]$. A related observation was pointed out in [27] for general kernel methods.

In short, one can interpret kernel ridge regression as the LMMSE estimator of a signal \mathbf{f} with covariance matrix equal to \mathbf{K} ; see also [28]. The LMMSE interpretation also suggests the usage of \mathbf{C} as a kernel matrix, which enables signal reconstruction even when the graph topology is unknown. Although this discussion hinges on kernel ridge regression after setting $\mathbf{K} = \mathbf{C}$, any other kernel estimator of the form (7) can benefit from vertex-covariance kernels too.

In most contemporary networks, sets of nodes may depend among each other via multiple types of relationships, which ordinary networks cannot capture [29]. Consequently, generalizing the traditional *single-layer* to *multilayer* networks that organize the nodes into different groups, called *layers*, is well motivated. For kernel-based approaches for function reconstruction over multilayer graphs see also [30].

2.3 Selecting kernels from a dictionary

The selection of the pertinent kernel matrix is of paramount importance to the performance of kernel-based methods [23, 31]. This section presents an MKL approach that effects kernel selection in graph signal reconstruction. Two algorithms with complementary strengths will be presented. Both rely on a user-specified *kernel dictionary*, and the best kernel is built from the dictionary in a data driven way.

The first algorithm, which we call *RKHS superposition*, is motivated by the fact that one specific \mathcal{H} in (6) is determined by some κ ; therefore, kernel selection is tantamount to RKHS selection. Consequently, a kernel dictionary $\{\kappa_m\}_{m=1}^M$ gives rise to a RKHS dictionary $\{\mathcal{H}_m\}_{m=1}^M$, which motivates estimates of the form³

$$\hat{f} = \sum_{m=1}^M \hat{f}_m, \quad \hat{f}_m \in \mathcal{H}_m. \quad (19)$$

Upon adopting a criterion that controls sparsity in this expansion, the “best” RKHSs will be selected. A reasonable approach is therefore to generalize (6)

³A sum is chosen here for tractability, but the right-hand side of (19) could in principle combine the functions $\{\hat{f}_m\}_m$ in different forms.

to accommodate multiple RKHSs. With \mathcal{L} selected to be the square loss and $\Omega(\zeta) = |\zeta|$, one can pursue an estimate \hat{f} by solving

$$\min_{\{f_m \in \mathcal{H}_m\}_{m=1}^M} \frac{1}{S} \sum_{s=1}^S \left[y_s - \sum_{m=1}^M f_m(v_{n_s}) \right]^2 + \mu \sum_{m=1}^M \|f_m\|_{\mathcal{H}_m}. \quad (20)$$

Invoking the representer theorem per f_m establishes that the minimizers of (20) can be written as

$$\hat{f}_m(v) = \sum_{s=1}^S \bar{\alpha}_s^m \kappa_m(v, v_{n_s}), \quad m = 1, \dots, M \quad (21)$$

for some coefficients $\bar{\alpha}_s^m$. Substituting (21) into (20) suggests obtaining these coefficients as

$$\arg \min_{\{\bar{\alpha}_m\}_{m=1}^M} \frac{1}{S} \left\| \mathbf{y} - \sum_{m=1}^M \bar{\mathbf{K}}_m \bar{\alpha}_m \right\|^2 + \mu \sum_{m=1}^M (\bar{\alpha}_m^T \bar{\mathbf{K}}_m \bar{\alpha}_m)^{1/2} \quad (22)$$

where $\bar{\alpha}_m := [\bar{\alpha}_1^m, \dots, \bar{\alpha}_S^m]^T$, and $\bar{\mathbf{K}}_m := \mathbf{S} \mathbf{K}_m \mathbf{S}^T$ with $(\mathbf{K}_m)_{n,n'} := \kappa_m(v_n, v_{n'})$. Letting $\check{\alpha}_m := \bar{\mathbf{K}}_m^{-1/2} \bar{\alpha}_m$, expression (22) becomes

$$\arg \min_{\{\check{\alpha}_m\}_{m=1}^M} \frac{1}{S} \left\| \mathbf{y} - \sum_{m=1}^M \bar{\mathbf{K}}_m^{1/2} \check{\alpha}_m \right\|^2 + \mu \sum_{m=1}^M \|\check{\alpha}_m\|_2. \quad (23)$$

Interestingly, (23) can be efficiently solved using the alternating-direction method of multipliers (ADMM) [32,33] after some nessecary reformulation [23].

After obtaining $\{\check{\alpha}_m\}_{m=1}^M$, the sought-after function estimate can be recovered as

$$\hat{\mathbf{f}} = \sum_{m=1}^M \mathbf{K}_m \mathbf{S}^T \bar{\alpha}_m = \sum_{m=1}^M \mathbf{K}_m \mathbf{S}^T \bar{\mathbf{K}}_m^{-1/2} \check{\alpha}_m. \quad (24)$$

This MKL algorithm can identify the best subset of RKHSs – and therefore kernels – but entails MS unknowns (cf. (22)). Next, an alternative approach is discussed which can reduce the number of variables to $M + S$ at the price of not being able to assure a sparse kernel expansion.

The alternative approach is to postulate a kernel of the form $\mathbf{K}(\boldsymbol{\theta}) = \sum_{m=1}^M \theta_m \mathbf{K}_m$, where $\{\mathbf{K}_m\}_{m=1}^M$ is given and $\theta_m \geq 0 \forall m$. The coefficients $\boldsymbol{\theta} := [\theta_1, \dots, \theta_M]^T$ can be found by jointly minimizing (12) with respect to $\boldsymbol{\theta}$ and $\bar{\boldsymbol{\alpha}}$ [34]

$$(\boldsymbol{\theta}, \hat{\bar{\boldsymbol{\alpha}}}) := \arg \min_{\boldsymbol{\theta}, \bar{\boldsymbol{\alpha}}} \frac{1}{S} \mathcal{L}(\mathbf{v}, \mathbf{y}, \bar{\mathbf{K}}(\boldsymbol{\theta}) \bar{\boldsymbol{\alpha}}) + \mu \Omega((\bar{\boldsymbol{\alpha}}^T \bar{\mathbf{K}}(\boldsymbol{\theta}) \bar{\boldsymbol{\alpha}})^{1/2}) \quad (25)$$

where $\bar{\mathbf{K}}(\boldsymbol{\theta}) := \mathbf{S} \mathbf{K}(\boldsymbol{\theta}) \mathbf{S}^T$. Except for degenerate cases, problem (25) is not jointly convex in $\boldsymbol{\theta}$ and $\hat{\bar{\boldsymbol{\alpha}}}$, but it is separately convex in each vector for a convex \mathcal{L} [34]. Iterative algorithms for solving (23) and (25) are available in [23].

2.4 Semi-parametric reconstruction

The approaches discussed so far are applicable to various problems but they are certainly limited by the modeling assumptions they make. In particular, the performance of algorithms belonging to the parametric family [11, 15, 35] is restricted by how well the signals actually adhere to the selected model. Non-parametric models on the other hand [2, 3, 6, 36], offer flexibility and robustness but they cannot readily incorporate information available a priori.

In practice however, it is not uncommon that neither of these approaches alone suffices for reliable inference. Consider, for instance, an employment-oriented social network such as LinkedIn, and suppose the goal is to estimate the salaries of all users given information about the salaries of a few. Clearly, besides network connections, exploiting available information regarding the users' education level and work experience could benefit the reconstruction task. The same is true in problems arising in link analysis, where the exploitation of Web's hierarchical structure can aid the task of estimating the importance of Web pages [37]. In recommender systems, inferring preference scores for every item, given the users' feedback about particular items, could be cast as a signal reconstruction problem over the item correlation graph. Data sparsity imposes severe limitations in the quality of pure collaborative filtering methods [38]. Exploiting side information about the items, is known to alleviate such limitations [39], leading to considerably improved recommendation performance [40, 41].

A promising direction to endow nonparametric methods with prior information relies on a *semi-parametric* approach whereby the signal of interest is modeled as the superposition of a parametric and a nonparametric component [42]. While the former leverages side information, the latter accounts for deviations from the parametric part, and can also promote smoothness using kernels on graphs. In this section we outline two simple and reliable semi-parametric estimators with complementary strengths, as detailed in [42].

2.4.1 Semi-parametric Inference

Function f is modeled as the superposition⁴

$$\mathbf{f} = \mathbf{f}_P + \mathbf{f}_{NP} \quad (26)$$

where $\mathbf{f}_P := [f_P(v_1), \dots, f_P(v_N)]^T$, and $\mathbf{f}_{NP} := [f_{NP}(v_1), \dots, f_{NP}(v_N)]^T$.

The parametric term $f_P(v) := \sum_{m=1}^M \beta_m b_m(v)$ captures the known signal structure via the basis $\mathcal{B} := \{b_m\}_{m=1}^M$, while the nonparametric term f_{NP} belongs to an RKHS \mathcal{H} , which accounts for deviations from the span of \mathcal{B} . The goal of this section is efficient and reliable estimation of \mathbf{f} given \mathbf{y} , \mathbf{S} , \mathcal{B} , \mathcal{H} and \mathcal{G} .

Since $f_{NP} \in \mathcal{H}$, vector \mathbf{f}_{NP} can be represented as in (3). By defining $\boldsymbol{\beta} := [\beta_1, \dots, \beta_M]^T$, and the $N \times M$ matrix \mathbf{B} with entries $(\mathbf{B})_{n,m} := b_m(v_n)$,

⁴for simplicity here we consider only the case of semi-parametric partially linear models.

the parametric term can be written in vector form as $\mathbf{f}_P := \mathbf{B}\boldsymbol{\beta}$. The semi-parametric estimates can be found as the solution of the following optimization problem

$$\begin{aligned} \{\hat{\boldsymbol{\alpha}}, \hat{\boldsymbol{\beta}}\} &= \arg \min_{\boldsymbol{\alpha}, \boldsymbol{\beta}} \frac{1}{S} \sum_{s=1}^S \mathcal{L}(y_s, f(v_{n_s})) + \mu \|f_{\text{NP}}\|_{\mathcal{H}}^2 \\ \text{s.t.} \quad &\mathbf{f} = \mathbf{B}\boldsymbol{\beta} + \mathbf{K}\boldsymbol{\alpha} \end{aligned} \quad (27)$$

where the fitting loss \mathcal{L} quantifies the deviation of f from the data, and $\mu > 0$ is the regularization scalar that controls overfitting the nonparametric term. Using (27), the semi-parametric estimates are expressed as $\hat{\mathbf{f}} = \mathbf{B}\hat{\boldsymbol{\beta}} + \mathbf{K}\hat{\boldsymbol{\alpha}}$.

Solving (27) entails minimization over $N + M$ variables. Clearly, when dealing with large-scale graphs this could lead to prohibitively large computational cost. To reduce complexity, the semi-parametric version of the representer theorem [18, 19] is employed, which establishes that

$$\hat{\mathbf{f}} = \mathbf{B}\hat{\boldsymbol{\beta}} + \mathbf{K}\mathbf{S}^T \hat{\boldsymbol{\alpha}} \quad (28)$$

where $\hat{\boldsymbol{\alpha}} := [\hat{\alpha}_1, \dots, \hat{\alpha}_S]^T$. Estimates $\hat{\boldsymbol{\alpha}}, \hat{\boldsymbol{\beta}}$ are found as

$$\begin{aligned} \{\hat{\boldsymbol{\alpha}}, \hat{\boldsymbol{\beta}}\} &= \arg \min_{\boldsymbol{\alpha}, \boldsymbol{\beta}} \frac{1}{S} \sum_{s=1}^S \mathcal{L}(y_s, f(v_{n_s})) + \mu \|f_{\text{NP}}\|_{\mathcal{H}}^2 \\ \text{s.t.} \quad &\mathbf{f} = \mathbf{B}\boldsymbol{\beta} + \mathbf{K}\mathbf{S}^T \boldsymbol{\alpha} \end{aligned} \quad (29)$$

where $\bar{\boldsymbol{\alpha}} := [\bar{\alpha}_1, \dots, \bar{\alpha}_S]^T$. The RKHS norm in (29) is expressed as $\|f_{\text{NP}}\|_{\mathcal{H}}^2 = \bar{\boldsymbol{\alpha}}^T \bar{\mathbf{K}} \bar{\boldsymbol{\alpha}}$, with $\bar{\mathbf{K}} := \mathbf{S}\mathbf{K}\mathbf{S}^T$. Relative to (27), the number of optimization variables in (29) is reduced to the more affordable $S + M$, with $S \ll N$.

Next, two loss functions with complementary benefits will be considered: the *square* loss and the *ϵ -insensitive* loss. The square loss function is

$$\mathcal{L}(y_s, f(v_{n_s})) := \|y_s - f(v_{n_s})\|_2^2 \quad (30)$$

and (29) admits the following closed-form solution

$$\hat{\boldsymbol{\alpha}} = (\mathbf{P}\bar{\mathbf{K}} + \mu \mathbf{I}_S)^{-1} \mathbf{P}\mathbf{y} \quad (31a)$$

$$\hat{\boldsymbol{\beta}} = (\bar{\mathbf{B}}^T \bar{\mathbf{B}})^{-1} \bar{\mathbf{B}}^T (\mathbf{y} - \bar{\mathbf{K}} \hat{\boldsymbol{\alpha}}) \quad (31b)$$

where $\bar{\mathbf{B}} := \mathbf{S}\mathbf{B}$, $\mathbf{P} := \mathbf{I}_S - \bar{\mathbf{B}}(\bar{\mathbf{B}}^T \bar{\mathbf{B}})^{-1} \bar{\mathbf{B}}^T$. The complexity of (31) is $\mathcal{O}(S^3 + M^3)$.

The *ϵ -insensitive* loss function is given by

$$\mathcal{L}(y_s, f(v_{n_s})) := \max(0, |y_s - f(v_{n_s})| - \epsilon) \quad (32)$$

where ϵ is tuned, e.g. via cross-validation, to minimize the generalization error and has well-documented merits in signal estimation from quantized data [43]. Substituting (32) into (29) yields a convex non-smooth quadratic problem that can be solved efficiently for $\hat{\boldsymbol{\alpha}}$ and $\hat{\boldsymbol{\beta}}$ using e.g. interior-point methods [18].

2.5 Numerical tests

This section reports on the signal reconstruction performance of different methods using real as well as synthetic data. The performance of the estimators is assessed via Monte Carlo simulation by comparing the normalized mean-square error (NMSE)

$$\text{NMSE} = \mathbb{E} \left[\frac{\|\hat{\mathbf{f}} - \mathbf{f}\|^2}{\|\mathbf{f}\|^2} \right]. \quad (33)$$

Multi-kernel reconstruction. The first data set contains departure and arrival information for flights among U.S. airports [44], from which 3×10^6 flights in the months of July, August, and September of 2014 and 2015 were selected. We construct a graph with $N = 50$ vertices corresponding to the airports with highest traffic, and whenever the number of flights between the two airports exceeds 100 within the observation window, we connect the corresponding nodes with an edge.

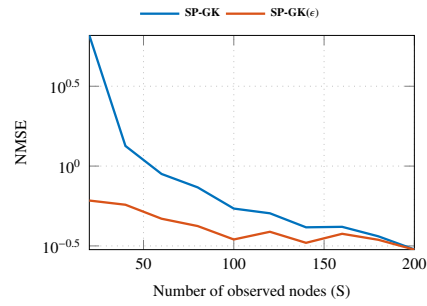
A signal was constructed per day averaging the arrival delay of *all* inbound flights per selected airport. A total of 184 signals were considered, of which the first 154 were used for training (July, August, September 2014, and July, August 2015), and the remaining 30 for testing (September 2015). The weights of the edges between airports were learned using the training data based on the technique described in [23].

	NMSE	RMSE[<i>min</i>]	
	KRR with cov. Kernel	0.34	3.95
Multi-Kernel Reconstruction	Multi-kernel, RS	0.44	4.51
	Multi-kernel, KS	0.43	4.45
	BL for B=2	1.55	8.45
	BL for B=3	32.64	38.72
	BL, cut-off	3.97	13.5

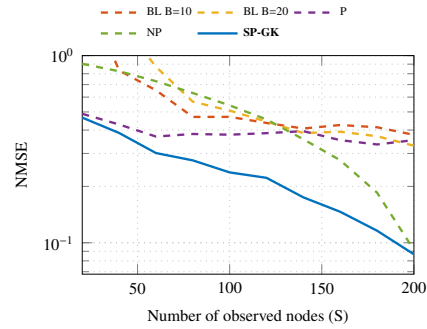
Table 2: Multi-Kernel Reconstruction

Table 2 lists the NMSE and the RMSE in minutes for the task of predicting the arrival delay at 40 airports when the delay at a randomly selected collection of 10 airports is observed. The second row corresponds to the ridge regression estimator that uses the nearly-optimal *estimated* covariance kernel. The next two rows correspond to the multi-kernel approaches in §2.3 with a dictionary of 30 diffusion kernels with values of σ^2 uniformly spaced between 0.1 and 7. The rest of the rows pertain to graph-bandlimited estimators (BL). Table 2 demonstrates the reliable performance of covariance kernels as well as the herein discussed multi-kernel approaches relative to competing alternatives.

NMSE of the synthetic signal estimates.



(a) ($\mu = 5 \times 10^{-4}$, $\sigma = 5 \times 10^{-4}$, $\text{SNR}_e = 5\text{dB}$).



(b) ($\mu = 5 \times 10^{-4}$, $\sigma = 5 \times 10^{-4}$, $\epsilon = 10^{-4}$, and $\text{SNR}_o = -5\text{dB}$).

Figure 1: NMSE of the synthetic signal estimates.

Semi-parametric reconstruction. An Erdős-Rényi graph with probability of edge presence 0.6 and $N = 200$ nodes was generated, and \mathbf{f} was formed by superimposing a bandlimited signal [13,15] plus a piecewise constant signal [45]; that is,

$$\mathbf{f} = \sum_{i=1}^{10} \gamma_i \mathbf{u}_i + \sum_{i=1}^6 \delta_i \mathbf{1}_{\mathcal{V}_i} \quad (34)$$

where $\{\gamma_i\}_{i=1}^{10}$ and $\{\delta_i\}_{i=1}^6$ are standardized Gaussian distributed; $\{\mathbf{u}_i\}_{i=1}^{10}$ are the eigenvectors associated with the 10 smallest eigenvalues of the Laplacian matrix; $\{\mathcal{V}_i\}_{i=1}^6$ are the vertex sets of 6 clusters obtained via spectral clustering [46]; and $\mathbf{1}_{\mathcal{V}_i}$ is the indicator vector with entries $(\mathbf{1}_{\mathcal{V}_i})_n := 1$, if $v_n \in \mathcal{V}_i$, and 0 otherwise. The parametric basis $\mathcal{B} = \{\mathbf{1}_{\mathcal{V}_i}\}_{i=1}^6$ was used by the estimators capturing the prior knowledge, and S vertices were sampled uniformly at random. The subsequent experiments evaluate the performance of the semi-parametric graph kernel estimators, SP-GK and SP-GK(ϵ) resulting from using (30) and (32) in (29), respectively; the *parametric* (P) that considers only the parametric term in (26); the *nonparametric* (NP) [2,3] that considers only the nonparametric term in (26); and the graph-bandlimited estimators (BL) from [13,15], which assume a bandlimited model with bandwidth B . For all the experiments, the diffusion kernel (cf. Table 1) with parameter σ is employed. First, white Gaussian noise e_s of variance σ_e^2 is added to each sample f_s to yield signal-to-noise ratio $\text{SNR}_e := \|\mathbf{f}\|_2^2 / (N\sigma_e^2)$. Fig. 1(b) presents the NMSE of different methods. As expected, the limited flexibility of the parametric approaches, BL and P, affects their ability to capture the true signal structure. The NP estimator achieves smaller NMSE, but only when the amount of available samples is adequate. Both semi-parametric estimators were found to outperform other approaches, exhibiting reliable reconstruction even with few samples.

To illustrate the benefits of employing different loss functions (30) and (32), we compare the performance of SP-GK and SP-GK(ϵ) in the presence of outlying noise. Each sample f_s is contaminated with Gaussian noise o_s of large variance σ_o^2 with probability $p = 0.1$. Fig. 1(a) demonstrates the robustness of SP-GK(ϵ) which is attributed to the ϵ -insensitive loss function (32). Further experiments using real signals can be found in [42].

3 Inference of dynamic functions over dynamic graphs

Networks that exhibit *time-varying connectivity* patterns with *time-varying node attributes* arise in a plethora of network science related applications. Sometimes these dynamic network topologies switch between a finite number of discrete states, governed by sudden changes of the underlying dynamics [47,48]. A challenging problem that arises in this setting is that of reconstructing time-evolving functions on graphs, given their values on a subset of vertices and time instants. Efficiently exploiting spatiotemporal dynamics can markedly impact sampling

costs by reducing the number of vertices that need to be observed to attain a target performance. Such a reduction can be of paramount importance in certain applications eg. in monitoring time-dependent activity of different regions of the brain through invasive electrocorticography (ECoG), where observing a vertex requires the implantation of an intracranial electrode [47].

Although one could reconstruct a time-varying function per time slot using the non- or semi-parametric methods of §2, leveraging time correlations typically yields estimators with improved performance. Schemes tailored for time-evolving functions on graphs include [49] and [50], which predict the function values at time t given observations up to time $t-1$. However, these schemes assume that the function of interest adheres to a specific vector autoregressive model. Other works target time-invariant functions, but can only afford tracking sufficiently slow variations. This is the case with the dictionary learning approach in [51] and the distributed algorithms in [52] and [53]. Unfortunately, the flexibility of these algorithms to capture spatial information is also limited since [51] focuses on Laplacian regularization, whereas [52] and [53] require the signal to be bandlimited.

Motivated by the aforementioned limitations, in what comes next we extend the framework presented in §2 accommodating time-varying function reconstruction over dynamic graphs. But before we delve into the time-varying setting, a few definitions are in order.

Definitions: A time-varying graph is a tuple $\mathcal{G}(t) := (\mathcal{V}, \mathbf{A}_t)$, where $\mathcal{V} := \{v_1, \dots, v_N\}$ is the vertex set, and $\mathbf{A}_t \in \mathbb{R}^{N \times N}$ is the adjacency matrix at time t , whose (n, n') -th entry $A_{n,n'}(t)$ assigns a weight to the pair of vertices $(v_n, v_{n'})$ at time t . A time-invariant graph is a special case with $\mathbf{A}_t = \mathbf{A}_{t'} \forall t, t'$. Adopting common assumptions made in related literature (e.g. [1, Ch. 2], [4, 9]), we also define $\mathcal{G}(t)$ (i) to have non-negative weights ($A_{n,n'}(t) \geq 0 \forall t$, and $\forall n \neq n'$); (ii) to have no self-edges ($A_{n,n}(t) = 0 \forall n, t$); and, (iii) to be undirected ($A_{n,n'}(t) = A_{n',n}(t) \forall n, n', t$).

A time-varying function or signal on a graph is a map $f : \mathcal{V} \times \mathcal{T} \rightarrow \mathbb{R}$, where $\mathcal{T} := \{1, 2, \dots\}$ is the set of time indices. The value $f(v_n, t)$ of f at vertex $v_n \in \mathcal{V}$ and time t , can be thought of as the value of an attribute of $v_n \in \mathcal{V}$ at time t . The values of f at time t will be collected in $\mathbf{f}_t := [f(v_1, t), \dots, f(v_N, t)]^T$.

At time t , vertices with indices in the time-dependent set $\mathcal{S}_t := \{n_1(t), \dots, n_{S(t)}(t)\}$, $1 \leq n_1(t) < \dots < n_{S(t)}(t) \leq N$, are observed. The resulting samples can be expressed as $y_s(t) = f(v_{n_s(t)}, t) + e_s(t)$, $s = 1, \dots, S(t)$, where $e_s(t)$ models observation error. By letting $\mathbf{y}_t := [y_1(t), \dots, y_{S(t)}(t)]^T$, the observations can be conveniently expressed as

$$\mathbf{y}_t = \mathbf{S}_t \mathbf{f}_t + \mathbf{e}_t, \quad t = 1, 2, \dots \quad (35)$$

where $\mathbf{e}_t := [e_1(t), \dots, e_{S(t)}(t)]^T$, and the $S(t) \times N$ sampling matrix \mathbf{S}_t contains ones at positions $(s, n_s(t))$, $s = 1, \dots, S(t)$ and zeros elsewhere.

The broad goal of this section is to “reconstruct” f from the observations $\{\mathbf{y}_t\}_t$ in (35). Two formulations will be considered.

Batch formulation. In the batch reconstruction problem, one aims at finding $\{\mathbf{f}_t\}_{t=1}^T$ given $\{\mathcal{G}(t)\}_{t=1}^T$, the sample locations $\{\mathbf{S}_t\}_{t=1}^T$, and all observations

$\{\mathbf{y}_t\}_{t=1}^T$.

Online formulation. At every time t , one is given \mathcal{G} together with \mathbf{S}_t and \mathbf{y}_t , and the goal is to find \mathbf{f}_t . The latter can be obtained possibly based on a previous estimate of \mathbf{f}_{t-1} , but the complexity per time slot t must be independent of t .

To solve these problems, we will rely on the assumption that f evolves smoothly over space and time, yet more structured dynamics can be incorporated if known.

3.1 Kernels on extended graphs

This section extends the kernel-based learning framework of §2 to subsume time-evolving functions over possibly dynamic graphs through the notion of *graph extension*, by which the time dimension receives the same treatment as the spatial dimension. The versatility of kernel-based methods to leverage spatial information [23] is thereby inherited and broadened to account for temporal dynamics as well. This vantage point also accommodates time-varying sampling sets and topologies.

3.1.1 Extended graphs

An immediate approach to reconstructing time-evolving functions is to apply (9) separately for each $t = 1, \dots, T$. This yields the instantaneous estimator (IE)

$$\hat{\mathbf{f}}_t^{(IE)} := \arg \min_{\mathbf{f}} \frac{1}{S(t)} \|\mathbf{y}_t - \mathbf{S}_t \mathbf{f}\|_2^2 + \mu \mathbf{f}^T \mathbf{K}_t^\dagger \mathbf{f}. \quad (36)$$

Unfortunately, this estimator does not account for the possible relation between e.g. $f(v_n, t)$ and $f(v_n, t-1)$. If, for instance, f varies slowly over time, an estimate of $f(v_n, t)$ may as well benefit from leveraging observations $y_s(\tau)$ at time instants $\tau \neq t$. Exploiting temporal dynamics potentially reduces the number of vertices that have to be sampled to attain a target reconstruction performance, which in turn can markedly reduce sampling costs.

Incorporating temporal dynamics into kernel-based reconstruction, which can only handle a single snapshot (cf. §2), necessitates an appropriate reformulation of time-evolving function reconstruction as a problem of reconstructing a time-invariant function. An appealing possibility is to replace \mathcal{G} with its *extended* version $\tilde{\mathcal{G}} := (\tilde{\mathcal{V}}, \tilde{\mathbf{A}})$, where each vertex in \mathcal{V} is replicated T times to yield the extended vertex set $\tilde{\mathcal{V}} := \{v_n(t), n = 1, \dots, N, t = 1, \dots, T\}$, and the $(n+N(t-1), n'+N(t'-1))$ -th entry of the $TN \times TN$ extended adjacency matrix $\tilde{\mathbf{A}}$ equals the weight of the edge $(v_n(t), v_{n'}(t'))$. The time-varying function f can thus be replaced with its extended time-invariant counterpart $\tilde{f} : \tilde{\mathcal{V}} \rightarrow \mathbb{R}$ with $\tilde{f}(v_n(t)) = f(v_n, t)$.

Definition 1. Let $\mathcal{V} := \{v_1, \dots, v_N\}$ denote a vertex set and let $\mathcal{G} := (\mathcal{V}, \{\mathbf{A}_t\}_{t=1}^T)$ be a time-varying graph. A graph $\tilde{\mathcal{G}}$ with vertex set $\tilde{\mathcal{V}} := \{v_n(t), n = 1, \dots, N, t = 1, \dots, T\}$ and $TN \times TN$ adjacency matrix $\tilde{\mathbf{A}}$ is an *extended graph* of \mathcal{G} if the t -th $N \times N$ diagonal block of $\tilde{\mathbf{A}}$ equals \mathbf{A}_t .

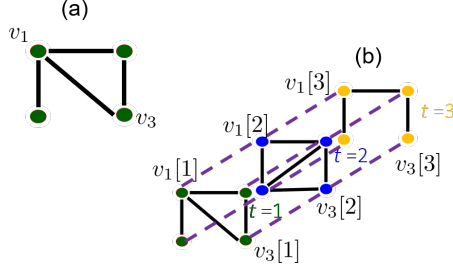


Figure 2: (a)Original graph (b) Extended graph $\tilde{\mathcal{G}}$ for diagonal $\mathbf{B}_t^{(T)}$. Edges connecting vertices at the same time instant are represented by solid lines whereas edges connecting vertices at different time instants are represented by dashed lines.

In general, the diagonal blocks $\{\mathbf{A}_t\}_{t=1}^T$ do not provide full description of the underlying extended graph. Indeed, one also needs to specify the off-diagonal block entries of $\tilde{\mathbf{A}}$ to capture the spatio-temporal dynamics of f .

As an example, consider an extended graph with

$$\tilde{\mathbf{A}} = \text{btridiag}\{\mathbf{A}_1, \dots, \mathbf{A}_T; \mathbf{B}_2^{(T)}, \dots, \mathbf{B}_T^{(T)}\} \quad (37)$$

where $\mathbf{B}_t^{(T)} \in \mathbb{R}_+^{N \times N}$ connects $\{v_n(t-1)\}_{n=1}^N$ to $\{v_n(t)\}_{n=1}^N$, $t = 2, \dots, T$ and $\text{btridiag}\{\mathbf{A}_1, \dots, \mathbf{A}_T; \mathbf{B}_2, \dots, \mathbf{B}_T\}$ represents the symmetric block tridiagonal matrix:

$$\tilde{\mathbf{A}} = \begin{bmatrix} \mathbf{A}_1 & \mathbf{B}_2^T & \mathbf{0} & \dots & \mathbf{0} & \mathbf{0} \\ \mathbf{B}_2 & \mathbf{A}_2 & \mathbf{B}_3^T & \dots & \mathbf{0} & \mathbf{0} \\ \mathbf{0} & \mathbf{B}_3 & \mathbf{A}_3 & \dots & \mathbf{0} & \mathbf{0} \\ \vdots & \vdots & \vdots & \ddots & \vdots & \vdots \\ \mathbf{0} & \mathbf{0} & \mathbf{0} & \dots & \mathbf{A}_{T-1} & \mathbf{B}_T^T \\ \mathbf{0} & \mathbf{0} & \mathbf{0} & \dots & \mathbf{B}_T & \mathbf{A}_T \end{bmatrix}.$$

For instance, each vertex can be connected to its neighbors at the previous time instant by setting $\mathbf{B}_t^{(T)} = \mathbf{A}_{t-1}$, or it can be connected to its replicas at adjacent time instants by setting $\mathbf{B}_t^{(T)}$ to be diagonal.

3.1.2 Batch and online reconstruction via space-time kernels

The extended graph enables a generalization of the estimators in §2 for time-evolving functions. The rest of this subsection discusses two such KRR estimators.

Consider first the batch formulation, where all the $\tilde{S} := \sum_{t=1}^T S_t$ samples in $\tilde{\mathbf{y}} := [\mathbf{y}_1^T, \dots, \mathbf{y}_T^T]^T$ are available, and the goal is to estimate $\tilde{\mathbf{f}} := [\mathbf{f}_1^T, \dots, \mathbf{f}_T^T]^T$. Directly applying the KRR criterion in (9) to reconstruct $\tilde{\mathbf{f}}$ on the extended graph $\tilde{\mathcal{G}}$ yields

$$\hat{\tilde{\mathbf{f}}} := \arg \min_{\tilde{\mathbf{f}}} \|\tilde{\mathbf{y}} - \tilde{\mathbf{S}}\tilde{\mathbf{f}}\|_{\tilde{\mathbf{D}}}^2 + \mu \tilde{\mathbf{f}}^T \tilde{\mathbf{K}} \tilde{\mathbf{f}} \quad (38a)$$

where $\tilde{\mathbf{K}}$ is now a $TN \times TN$ “space-time” kernel matrix,

$\tilde{\mathbf{S}} := \text{bdiag}\{\mathbf{S}_1, \dots, \mathbf{S}_T\}$, and $\mathbf{D} := \text{bdiag}\{S(1)\mathbf{I}_{S(1)}, \dots, S(T)\mathbf{I}_{S(T)}\}$. If $\tilde{\mathbf{K}}$ is invertible, (38a) can be solved in closed form as

$$\hat{\mathbf{f}} = \tilde{\mathbf{K}}\tilde{\mathbf{S}}^T(\tilde{\mathbf{S}}\tilde{\mathbf{K}}\tilde{\mathbf{S}}^T + \mu\mathbf{D})^{-1}\tilde{\mathbf{y}}. \quad (38b)$$

The “space-time” kernel $\tilde{\mathbf{K}}$, captures complex spatiotemporal dynamics. If the topology is time invariant, $\tilde{\mathbf{K}}$ can be specified in a bidimensional plane of spatio-temporal frequency similar to §2.2⁵.

In the online formulation, one aims to estimate \mathbf{f}_t after the $\tilde{S}(t) := \sum_{\tau=1}^t S(\tau)$ samples in $\tilde{\mathbf{y}}_t := [\mathbf{y}_1^T, \dots, \mathbf{y}_t^T]^T$ become available. Based on these samples, the KRR estimate of $\tilde{\mathbf{f}}$, denoted as $\hat{\mathbf{f}}_{1:T|t}$, is clearly

$$\hat{\mathbf{f}}_{1:T|t} := \arg \min_{\tilde{\mathbf{f}}} \|\tilde{\mathbf{y}}_t - \tilde{\mathbf{S}}_t \tilde{\mathbf{f}}\|_{\mathbf{D}_t}^2 + \mu \tilde{\mathbf{f}}^T \tilde{\mathbf{K}}^{-1} \tilde{\mathbf{f}} \quad (39a)$$

$$= \tilde{\mathbf{K}}\tilde{\mathbf{S}}_t^T(\tilde{\mathbf{S}}_t\tilde{\mathbf{K}}\tilde{\mathbf{S}}_t^T + \mu\mathbf{D}_t)^{-1}\tilde{\mathbf{y}}_t. \quad (39b)$$

where $\tilde{\mathbf{K}}$ is assumed invertible for simplicity, $\mathbf{D}_t := \text{bdiag}\{S(1)\mathbf{I}_{S(1)}, \dots, S(t)\mathbf{I}_{S(t)}\}$, and $\tilde{\mathbf{S}}_t := [\text{diag}\{\mathbf{S}_1, \dots, \mathbf{S}_t\}, \mathbf{0}_{\tilde{S}(t) \times (T-t)N}] \in \{0, 1\}^{\tilde{S}(t) \times TN}$.

The estimate in (39) comprises the per slot estimates $\{\hat{\mathbf{f}}_{\tau|t}\}_{\tau=1}^T$; that is, $\hat{\mathbf{f}}_{1:T|t} := [\hat{\mathbf{f}}_{1|t}^T, \dots, \hat{\mathbf{f}}_{T|t}^T]^T$ with $\hat{\mathbf{f}}_{\tau|t} := [\hat{f}_1(\tau|t), \dots, \hat{f}_N(\tau|t)]^T$, where $\hat{\mathbf{f}}_{\tau|t}$ (respectively $\hat{f}_n(\tau|t)$) is the KRR estimate of \mathbf{f}_τ ($f(v_n, \tau)$) given the observations up to time t . With this notation, it follows that for all t, τ

$$\hat{\mathbf{f}}_{\tau|t} = (\mathbf{i}_{T,\tau}^T \otimes \mathbf{I}_N) \hat{\mathbf{f}}_{1:T|t}. \quad (40)$$

Regarding t as the present, (39) therefore provides estimates of past, present, and future values of f . The solution to the online problem comprises the sequence of *present* KRR estimates for all t , that is, $\{\hat{\mathbf{f}}_{t|t}\}_{t=1}^T$. This can be obtained by solving (39a) in closed form per t as in (39b), and then applying (40). However, such an approach does not yield a desirable online algorithm since its complexity per time slot is $\mathcal{O}(\tilde{S}^3(t))$, and therefore increasing with t . For this reason, this approach is not satisfactory since the online problem formulation requires the complexity per time slot of the desired algorithm to be independent of t . An algorithm that does satisfy this requirement yet provides the exact KRR estimate is presented next when the kernel matrix is any positive definite matrix $\tilde{\mathbf{K}}$ satisfying

$$\tilde{\mathbf{K}}^{-1} = \text{btridiag}\{\mathbf{D}_1, \dots, \mathbf{D}_T; \mathbf{C}_2, \dots, \mathbf{C}_T\} \quad (41)$$

for some $N \times N$ matrices $\{\mathbf{D}_t\}_{t=1}^T$ and $\{\mathbf{C}_t\}_{t=2}^T$. Kernels in this important family are designed in [54].

⁵For general designs of space-time kernels $\tilde{\mathbf{K}}$ for time-invariant as well as time-varying topologies see [54].

Algorithm 1: Recursion to set the parameters of the KKF

Input: $\mathbf{D}_t, t = 1, \dots, T, \mathbf{C}_t, t = 2, \dots, T$.

1: **Set** $\Sigma_T^{-1} = \mathbf{D}_T$

2: **for** $t = T, T - 1, \dots, 2$ **do**

3: $\mathbf{P}_t = -\Sigma_t \mathbf{C}_t$

4: $\Sigma_{t-1}^{-1} = \mathbf{D}_{t-1} - \mathbf{P}_t^T \Sigma_t^{-1} \mathbf{P}_t$

Output: $\Sigma_t, t = 1, \dots, T, \mathbf{P}_t, t = 2, \dots, T$

If $\tilde{\mathbf{K}}$ is of the form (41) then the kernel Kalman filter (KKF) in Algorithm 2 returns the sequence $\{\hat{\mathbf{f}}_{t|t}\}_{t=1}^T$, where $\hat{\mathbf{f}}_{t|t}$ is given by (40). The $N \times N$ matrices $\{\mathbf{P}_\tau\}_{\tau=2}^T$ and $\{\Sigma_\tau\}_{\tau=1}^T$ are obtained offline by Algorithm 1, and $\sigma_e^2(\tau) = \mu S(\tau) \forall \tau$.

The KKF generalizes the probabilistic KF since the latter is recovered upon setting $\tilde{\mathbf{K}}$ to be the covariance matrix of $\tilde{\mathbf{f}}$ in the probabilistic KF. The assumptions made by the probabilistic KF are stronger than those involved in the KKF. Specifically, in the probabilistic KF, \mathbf{f}_t must adhere to a linear state-space model, $\mathbf{f}_t = \mathbf{P}_t \mathbf{f}_{t-1} + \boldsymbol{\eta}_t$, with known transition matrix \mathbf{P}_t , where the state noise $\boldsymbol{\eta}_t$ is uncorrelated over time and has known covariance matrix Σ_t . Furthermore, the observation noise \mathbf{e}_t must be uncorrelated over time and have known covariance matrix. Correspondingly, the performance guarantees of the probabilistic KF are also stronger: the resulting estimate is optimal in the mean-square error sense among all linear estimators. Furthermore, if $\boldsymbol{\eta}_t$ and \mathbf{y}_t are jointly Gaussian, $t = 1, \dots, T$, then the probabilistic KF estimate is optimal in the mean-square error sense among all (not necessarily linear) estimators. In contrast, the requirements of the proposed KKF are much weaker since they only specify that f must evolve smoothly with respect to a given extended graph. As expected, the performance guarantees are similarly weaker; see e.g. [18, Ch. 5]. However, since the KKF generalizes the probabilistic KF, the reconstruction performance of the former for judiciously selected $\tilde{\mathbf{K}}$ cannot be worse than the reconstruction performance of the latter for any given criterion. The caveat, however, is that such a selection is not necessarily easy.

For the rigorous statement and proof relating the celebrated KF [55, Ch. 17] and the optimization problem in (39a), see [54]. Algorithm 2 requires $\mathcal{O}(N^3)$ operations per time slot, whereas the complexity of evaluating (39b) for the t -th time slot is $\mathcal{O}(\tilde{S}^3(t))$, which increases with t and becomes eventually prohibitive. Since distributed versions of the Kalman filter are well studied [56], decentralized KKF algorithms can be pursued to further reduce the computational complexity.

3.2 Multi-kernel kriged Kalman filters

The following section applies the KRR framework presented in §2 to online data-adaptive estimators of \mathbf{f}_t . Specifically, a spatio-temporal model is presented that judiciously captures the dynamics over space and time. Based on this model the KRR criterion over time and space is formulated, and an online algorithm

Algorithm 2: Kernel Kalman filter (KKF)

Input: $\{\Sigma_t \in \mathbb{S}_+^N\}_{t=1}^T$, $\{\mathbf{P}_t \in \mathbb{R}^{N \times N}\}_{t=2}^T$,
 $\{\mathbf{y}_t \in \mathbb{R}^{S(t)}\}_{t=1}^T$, $\{\mathbf{S}_t \in \{0, 1\}^{S(t) \times N}\}_{t=1}^T$,
 $\{\sigma_e^2(t) > 0\}_{t=1}^T$.

- 1: Set $\hat{\mathbf{f}}_{0|0} = \mathbf{0}$, $\mathbf{M}_{0|0} = \mathbf{0}$, $\mathbf{P}_1 = \mathbf{0}$
- 2: for $t = 1, \dots, T$ do
- 3: $\hat{\mathbf{f}}_{t|t-1} = \mathbf{P}_t \hat{\mathbf{f}}_{t-1|t-1}$
- 4: $\mathbf{M}_{t|t-1} = \mathbf{P}_t \mathbf{M}_{t-1|t-1} \mathbf{P}_t^T + \Sigma_t$
- 5: $\mathbf{G}_t = \mathbf{M}_{t|t-1} \mathbf{S}_t^T (\sigma_e^2(t) \mathbf{I} + \mathbf{S}_t \mathbf{M}_{t|t-1} \mathbf{S}_t^T)^{-1}$
- 6: $\hat{\mathbf{f}}_{t|t} = \hat{\mathbf{f}}_{t|t-1} + \mathbf{G}_t (\mathbf{y}_t - \mathbf{S}_t \hat{\mathbf{f}}_{t|t-1})$
- 7: $\mathbf{M}_{t|t} = (\mathbf{I} - \mathbf{G}_t \mathbf{S}_t) \mathbf{M}_{t|t-1}$

Output: $\hat{\mathbf{f}}_{t|t}$, $t = 1, \dots, T$; \mathbf{M}_t , $t = 1, \dots, T$.

is derived with affordable computational complexity, when the kernels are pre-selected. To bypass the need for selecting an appropriate kernel, this section discusses a data-adaptive multi-kernel learning extension of the KRR estimator that learns the optimal kernel “on-the-fly.”

3.2.1 Spatio-temporal models

Consider modeling the dynamics of \mathbf{f}_t separately over time and space as $f(v_n, t) = f^{(\nu)}(v_n, t) + f^{(x)}(v_n, t)$, or in vector form

$$\mathbf{f}_t = \mathbf{f}_t^{(\nu)} + \mathbf{f}_t^{(x)} \quad (42)$$

where $\mathbf{f}_t^{(\nu)} := [f^{(\nu)}(v_1, t), \dots, f^{(\nu)}(v_N, t)]^T$ and $\mathbf{f}_t^{(x)} := [f^{(x)}(v_1, t), \dots, f^{(x)}(v_N, t)]^T$. The first term $\{\mathbf{f}_t^{(\nu)}\}_t$ captures only spatial dependencies, and can be thought of as exogenous input to the graph that does not affect the evolution of the function in time.

The second term $\{\mathbf{f}_t^{(x)}\}_t$ accounts for spatio-temporal dynamics. A popular approach [57, Ch. 3] models $\mathbf{f}_t^{(x)}$ with the state equation

$$\mathbf{f}_t^{(x)} = \mathbf{A}_{t,t-1} \mathbf{f}_{t-1}^{(x)} + \boldsymbol{\eta}_t, \quad t = 1, 2, \dots \quad (43)$$

where $\mathbf{A}_{t,t-1}$ is a generic transition matrix that can be chosen e.g. as the $N \times N$ adjacency of a possibly directed “transition graph,” with $\mathbf{f}_0^{(x)} = \mathbf{0}$, and $\boldsymbol{\eta}_t \in \mathbb{R}^N$ capturing the state error. The state transition matrix $\mathbf{A}_{t,t-1}$ can be selected in accordance with the prior information available. Simplicity in estimation motivates the random walk model [58], where $\mathbf{A}_{t,t-1} = \alpha \mathbf{I}_N$ with $\alpha > 0$. On the other hand, adherence to the graph, prompts the selection $\mathbf{A}_{t,t-1} = \alpha \mathbf{A}$, in which case (43) amounts to a diffusion process on the time-invariant graph \mathcal{G} . The recursion in (43) is a vector autoregressive model (VARM) of order one, and offers flexibility in tracking multiple forms of temporal dynamics [57, Ch.

3]. The model in (43) captures the dependence between $f^{(x)}(v_n, t)$ and its time lagged versions $\{f^{(x)}(v_n, t-1)\}_{n=1}^N$.

Next, a model with increased flexibility is presented to account for instantaneous spatial dependencies as well

$$\mathbf{f}_t^{(x)} = \mathbf{A}_{t,t} \mathbf{f}_t^{(x)} + \mathbf{A}_{t,t-1} \mathbf{f}_{t-1}^{(x)} + \boldsymbol{\eta}_t, \quad t = 1, 2, \dots \quad (44)$$

where $\mathbf{A}_{t,t}$ encodes the instantaneous relation between $f^{(x)}(v_n, t)$ and $\{f^{(x)}(v_{n'}, t)\}_{n' \neq n}$. The recursion in (44) amounts to a structural vector autoregressive model (SVARM) [47]. Interestingly, (44) can be rewritten as

$$\mathbf{f}_t^{(x)} = (\mathbf{I}_N - \mathbf{A}_{t,t})^{-1} \mathbf{A}_{t,t-1} \mathbf{f}_{t-1}^{(x)} + (\mathbf{I}_N - \mathbf{A}_{t,t})^{-1} \boldsymbol{\eta}_t \quad (45)$$

where $\mathbf{I}_N - \mathbf{A}_{t,t}$ is assumed invertible. After defining $\tilde{\boldsymbol{\eta}}_t := (\mathbf{I}_N - \mathbf{A}_{t,t})^{-1} \boldsymbol{\eta}_t$ and $\tilde{\mathbf{A}}_{t,t-1} := (\mathbf{I}_N - \mathbf{A}_{t,t})^{-1} \mathbf{A}_{t,t-1}$, (44) boils down to

$$\mathbf{f}_t^{(x)} = \tilde{\mathbf{A}}_{t,t-1} \mathbf{f}_{t-1}^{(x)} + \tilde{\boldsymbol{\eta}}_t \quad (46)$$

which is equivalent to (43). This section will focus on deriving estimators based on (43), but can also accommodate (44) using the aforementioned reformulation.

Modeling \mathbf{f}_t as the superposition of a term $\mathbf{f}_t^{(x)}$ capturing the slow dynamics over time with a state space equation, and a term $\mathbf{f}_t^{(\nu)}$ accounting for fast dynamics is motivated by the application at hand [58–60]. In the kriging terminology [59], $\mathbf{f}_t^{(\nu)}$ is said to model small-scale *spatial fluctuations*, whereas $\mathbf{f}_t^{(x)}$ captures the so-called *trend*. The decomposition (42) is often dictated by the sampling interval: while $\mathbf{f}_t^{(x)}$ captures slow dynamics relative to the sampling interval, fast variations are modeled with $\mathbf{f}_t^{(\nu)}$. Such a modeling approach is motivated in the prediction of network delays [58], where $\mathbf{f}_t^{(x)}$ represents the queuing delay while $\mathbf{f}_t^{(\nu)}$ the propagation, transmission, and processing delays. Likewise, when predicting prices across different stocks, $\mathbf{f}_t^{(x)}$ captures the daily evolution of the stock market, which is correlated across stocks and time samples, while $\mathbf{f}_t^{(\nu)}$ describes unexpected changes, such as the daily drop of the stock market due to political statements, which are assumed uncorrelated over time.

3.2.2 Kernel kriged Kalman filter

The spatio-temporal model in (42), (43) can represent multiple forms of spatio-temporal dynamics by judicious selection of the associated parameters. The *batch* KRR estimator over time yields

$$\begin{aligned} \arg \min_{\{\mathbf{f}_\tau^{(x)}, \boldsymbol{\eta}_\tau, \mathbf{f}_\tau^{(\nu)}, \mathbf{f}_\tau\}_{\tau=1}^t} & \sum_{\tau=1}^t \frac{1}{S(\tau)} \|\mathbf{y}_\tau - \mathbf{S}_\tau \mathbf{f}_\tau\|^2 + \mu_1 \sum_{\tau=1}^t \|\boldsymbol{\eta}_\tau\|_{\mathbf{K}^{(\eta)}}^2 + \mu_2 \sum_{\tau=1}^t \|\mathbf{f}_\tau^{(\nu)}\|_{\mathbf{K}^{(\nu)}}^2 \\ \text{s.t.} \quad & \boldsymbol{\eta}_\tau = \mathbf{f}_\tau^{(x)} - \mathbf{A}_{\tau,\tau-1} \mathbf{f}_{\tau-1}^{(x)}, \quad \mathbf{f}_\tau = \mathbf{f}_\tau^{(\nu)} + \mathbf{f}_\tau^{(x)}, \quad \tau = 1, \dots, t. \end{aligned} \quad (47)$$

The first term in (47) penalizes the fitting error in accordance with (1). The scalars $\mu_1, \mu_2 \geq 0$ are regularization parameters controlling the effect of the

kernel regularizers, while prior information about $\{\mathbf{f}_\tau^{(\nu)}, \boldsymbol{\eta}_\tau\}_{\tau=1}^t$ may guide the selection of the appropriate kernel matrices. The constraints in (47) imply adherence to (43) and (42). Since the $\mathbf{f}_\tau^{(\nu)}, \boldsymbol{\eta}_\tau$ are defined over the time-evolving $\mathcal{G}(\tau)$, a potential approach is to select Laplacian kernels as $\mathbf{K}_\tau^{(\nu)}, \mathbf{K}_\tau^{(\eta)}$, see §2.2. Next, we rewrite (47) in a form amenable to online solvers, namely

$$\begin{aligned} \arg \min_{\{\mathbf{f}_\tau^{(\chi)}, \mathbf{f}_\tau^{(\nu)}\}_{\tau=1}^t} & \sum_{\tau=1}^t \frac{1}{S(\tau)} \|\mathbf{y}_\tau - \mathbf{S}_\tau \mathbf{f}_\tau^{(\chi)} - \mathbf{S}_\tau \mathbf{f}_\tau^{(\nu)}\|^2 + \\ & + \mu_1 \sum_{\tau=1}^t \|\mathbf{f}_\tau^{(\chi)} - \mathbf{A}_{\tau, \tau-1} \mathbf{f}_{\tau-1}^{(\chi)}\|_{\mathbf{K}_\tau^{(\eta)}}^2 + \\ & + \mu_2 \sum_{\tau=1}^t \|\mathbf{f}_\tau^{(\nu)}\|_{\mathbf{K}_\tau^{(\nu)}}^2. \end{aligned} \quad (48)$$

In a batch form the optimization in (48) yields $\{\hat{\mathbf{f}}_{\tau|t}^{(\nu)}, \hat{\mathbf{f}}_{\tau|t}^{(\chi)}\}_{\tau=1}^t$ per slot t with complexity that grows with t . Fortunately, the *filtered* solutions $\{\hat{\mathbf{f}}_{\tau|\tau}^{(\nu)}, \hat{\mathbf{f}}_{\tau|\tau}^{(\chi)}\}_{\tau=1}^t$ of (48), are attained by the kernel kriged Kalman filter (KeKriKF) in an *online* fashion. For the proof the reader is referred to [61]. One iteration of the proposed KeKriKF is summarized as Algorithm 3. This online estimator – with computational complexity $\mathcal{O}(N^3)$ per t – tracks the temporal variations of the signal of interest through (43), and promotes desired properties such as smoothness over the graph, using $\mathbf{K}_t^{(\nu)}$ and $\mathbf{K}_t^{(\eta)}$. Different from existing KriKF approaches over graphs [58], the KeKriKF takes into account the underlying graph structure in estimating $\mathbf{f}_t^{(\nu)}$ as well as $\mathbf{f}_t^{(\chi)}$. Furthermore, by using \mathbf{L}_t in (16), it can also accommodate dynamic graph topologies. Finally, it should be noted that KeKriKF encompasses as a special case the KriKF, which relies on knowing the statistical properties of the function [58–60, 62].

Lack of prior information prompts the development of data-driven approaches that efficiently learn the appropriate kernel matrix. In the next section, we discuss an online MKL approach for achieving this goal.

3.2.3 Online multi-kernel Learning

To cope with lack of prior information about the pertinent kernel, the following dictionaries of kernels will be considered $\mathcal{D}_\nu := \{\mathbf{K}^{(\nu)}(m) \in \mathbb{S}_+^N\}_{m=1}^{M_\nu}$ and $\mathcal{D}_\eta := \{\mathbf{K}^{(\eta)}(m) \in \mathbb{S}_+^N\}_{m=1}^{M_\eta}$. For the following assume that $\mathbf{K}_\tau^{(\nu)} = \mathbf{K}^{(\nu)}$, $\mathbf{K}_\tau^{(\eta)} = \mathbf{K}^{(\eta)}$ and $\mathbf{S}_\tau = \mathbf{S}$, $\forall \tau$. Moreover, we postulate that the kernel matrices are of the form $\mathbf{K}^{(\nu)} = \mathbf{K}^{(\nu)}(\boldsymbol{\theta}^{(\nu)}) = \sum_{m=1}^{M_\nu} \theta^{(\nu)}(m) \mathbf{K}^{(\nu)}(m)$ and $\mathbf{K}^{(\eta)} = \mathbf{K}^{(\eta)}(\boldsymbol{\theta}^{(\eta)}) = \sum_{m=1}^{M_\eta} \theta^{(\eta)}(m) \mathbf{K}^{(\eta)}(m)$, where $\theta^{(\eta)}(m), \theta^{(\nu)}(m) \geq 0$, $\forall m$.

Next, in accordance with §2.3 the coefficients $\boldsymbol{\theta}^{(\nu)} = [\theta^{(\nu)}(1), \dots, \theta^{(\nu)}(M)]^T$ and $\boldsymbol{\theta}^{(\eta)} = [\theta^{(\eta)}(1), \dots, \theta^{(\eta)}(M)]^T$ can be found by jointly minimizing (48) with

Algorithm 3: Kernel Kriged Kalman filter (KeKriKF)

Input: $\mathbf{K}_t^{(\eta)}; \mathbf{K}_t^{(\nu)} \in \mathbb{S}_+^N; \mathbf{A}_{t,t-1} \in \mathbb{R}^{N \times N}; \mathbf{y}_t \in \mathbb{R}^{S(t)}; \mathbf{S}_t \in \{0, 1\}^{S(t) \times N}$.

- 1: $\bar{\mathbf{K}}_t^{(\chi)} = \frac{1}{\mu_2} \mathbf{S}_t \mathbf{K}_t^{(\nu)} \mathbf{S}_t^T + S(t) \mathbf{I}_{S(t)}$
- 2: $\hat{\mathbf{f}}_{t|t-1}^{(\chi)} = \mathbf{A}_{t,t-1} \hat{\mathbf{f}}_{t-1|t-1}^{(\chi)}$
- 3: $\mathbf{M}_{t|t-1} = \mathbf{A}_{t,t-1} \mathbf{M}_{t-1|t-1} \mathbf{A}_{t,t-1}^T + \frac{1}{\mu_1} \mathbf{K}_t^{(\eta)}$
- 4: $\mathbf{G}_t = \mathbf{M}_{t|t-1} \mathbf{S}_t^T (\bar{\mathbf{K}}_t^{(\chi)} + \mathbf{S}_t \mathbf{M}_{t|t-1} \mathbf{S}_t^T)^{-1}$
- 5: $\mathbf{M}_{t|t} = (\mathbf{I} - \mathbf{G}_t \mathbf{S}_t) \mathbf{M}_{t|t-1}$
- 6: $\hat{\mathbf{f}}_{t|t}^{(\chi)} = \hat{\mathbf{f}}_{t|t-1}^{(\chi)} + \mathbf{G}_t (\mathbf{y}_t - \mathbf{S}_t \hat{\mathbf{f}}_{t|t-1}^{(\chi)})$
- 7: $\hat{\mathbf{f}}_{t|t}^{(\nu)} = \mathbf{K}_t^{(\nu)} \mathbf{S}_t^T \bar{\mathbf{K}}_t^{(\chi)^{-1}} (\mathbf{y}_t - \mathbf{S}_t \hat{\mathbf{f}}_{t|t}^{(\chi)})$

Output: $\hat{\mathbf{f}}_{t|t}^{(\chi)}; \hat{\mathbf{f}}_{t|t}^{(\nu)}; \mathbf{M}_{t|t}$.

respect to $\{\mathbf{f}_\tau^{(\chi)}, \mathbf{f}_\tau^{(\nu)}\}_{\tau=1}^t, \boldsymbol{\theta}^{(\nu)}$ and $\boldsymbol{\theta}^{(\eta)}$ that yields

$$\begin{aligned} \arg \min_{\substack{\{\mathbf{f}_\tau^{(\chi)}, \mathbf{f}_\tau^{(\nu)}\}_{\tau=1}^t \\ \boldsymbol{\theta}^{(\nu)} \geq \mathbf{0}, \boldsymbol{\theta}^{(\eta)} \geq \mathbf{0}}} & \sum_{\tau=1}^t \frac{1}{S} \|\mathbf{y}_\tau - \mathbf{S} \mathbf{f}_\tau^{(\chi)} - \mathbf{S} \mathbf{f}_\tau^{(\nu)}\|^2 + \mu_1 \sum_{\tau=1}^t \|\mathbf{f}_\tau^{(\chi)} - \mathbf{A}_{\tau,\tau-1} \mathbf{f}_{\tau-1}^{(\chi)}\|_{\mathbf{K}^{(\eta)}(\boldsymbol{\theta}^{(\eta)})}^2 \\ & + \mu_2 \sum_{\tau=1}^t \|\mathbf{f}_\tau^{(\nu)}\|_{\mathbf{K}^{(\nu)}(\boldsymbol{\theta}^{(\nu)})}^2 + t \rho_\nu \|\boldsymbol{\theta}^{(\nu)}\|_2^2 + t \rho_\eta \|\boldsymbol{\theta}^{(\eta)}\|_2^2 \end{aligned} \quad (49)$$

where $\rho_\nu, \rho_\eta \geq 0$ are regularization parameters, that effect a ball constraint on $\boldsymbol{\theta}^{(\nu)}$ and $\boldsymbol{\theta}^{(\eta)}$, weighted by t to account for the first three terms that are growing with t . Observe that the optimization problem in (49) gives time varying estimates $\hat{\boldsymbol{\theta}}_t^{(\nu)}$ and $\hat{\boldsymbol{\theta}}_t^{(\eta)}$ allowing to track the optimal $\mathbf{K}^{(\nu)}$ and $\mathbf{K}^{(\eta)}$ that change over time respectively.

The optimization problem in (49) is not jointly convex in $\{\mathbf{f}_\tau^{(\chi)}, \mathbf{f}_\tau^{(\nu)}\}_{\tau=1}^t, \boldsymbol{\theta}^{(\nu)}, \boldsymbol{\theta}^{(\eta)}$, but it is separately convex in these variables. To solve (49) alternating minimization strategies will be employed, that suggest optimizing with respect to one variable, while keeping the other variables fixed [63]. If $\boldsymbol{\theta}^{(\nu)}, \boldsymbol{\theta}^{(\eta)}$ are considered fixed, (49) reduces to (48), which can be solved by Algorithm 3 for the estimates $\hat{\mathbf{f}}_{t|t}^{(\chi)}, \hat{\mathbf{f}}_{t|t}^{(\nu)}$ at each t . For $\{\mathbf{f}_\tau^{(\chi)}, \mathbf{f}_\tau^{(\nu)}\}_{\tau=1}^t$ fixed and replaced by $\{\hat{\mathbf{f}}_{\tau|\tau}^{(\chi)}, \hat{\mathbf{f}}_{\tau|\tau}^{(\nu)}\}_{\tau=1}^t$ in (48) the time-varying estimates of $\boldsymbol{\theta}^{(\nu)}, \boldsymbol{\theta}^{(\eta)}$ are found by

$$\hat{\boldsymbol{\theta}}_t^{(\eta)} = \arg \min_{\boldsymbol{\theta}^{(\eta)} \geq \mathbf{0}} \frac{1}{t} \sum_{\tau=1}^t \|\hat{\mathbf{f}}_{\tau|\tau}^{(\chi)} - \mathbf{A}_{\tau,\tau-1} \hat{\mathbf{f}}_{\tau-1|\tau-1}^{(\chi)}\|_{\mathbf{K}^{(\eta)}(\boldsymbol{\theta}^{(\eta)})}^2 + \frac{\rho_\eta}{\mu_1} \|\boldsymbol{\theta}^{(\eta)}\|_2^2 \quad (50a)$$

$$\hat{\boldsymbol{\theta}}_t^{(\nu)} = \arg \min_{\boldsymbol{\theta}^{(\nu)} \geq \mathbf{0}} \frac{1}{t} \sum_{\tau=1}^t \|\hat{\mathbf{f}}_{\tau|\tau}^{(\nu)}\|_{\mathbf{K}^{(\nu)}(\boldsymbol{\theta}^{(\nu)})}^2 + \frac{\rho_\nu}{\mu_2} \|\boldsymbol{\theta}^{(\nu)}\|_2^2. \quad (50b)$$

The optimization problems (50a) and (50b) are strongly convex and iterative algorithms are available based on projected gradient descent (PGD) [64], or the

Frank-Wolfe algorithm [65]. When the kernel matrices belong to the Laplacian family (16), efficient algorithms that exploit the common eigenspace of the kernels in the dictionary have been developed in [61]. The proposed method reduces the per step computational complexity of PGD from a prohibitive $\mathcal{O}(N^3M)$ for general kernels to a more affordable $\mathcal{O}(NM)$ for Laplacian kernels. The proposed algorithm, termed multi-kernel KriKF (MKriKF) alternates between computing $\hat{\mathbf{f}}_{t|t}^{(\chi)}$ and $\hat{\mathbf{f}}_{t|t}^{(\nu)}$ utilizing the KKriKF and estimating $\hat{\boldsymbol{\theta}}_t^{(\nu)}$ and $\hat{\boldsymbol{\theta}}_t^{(\eta)}$ from solving (50b) and (50a).

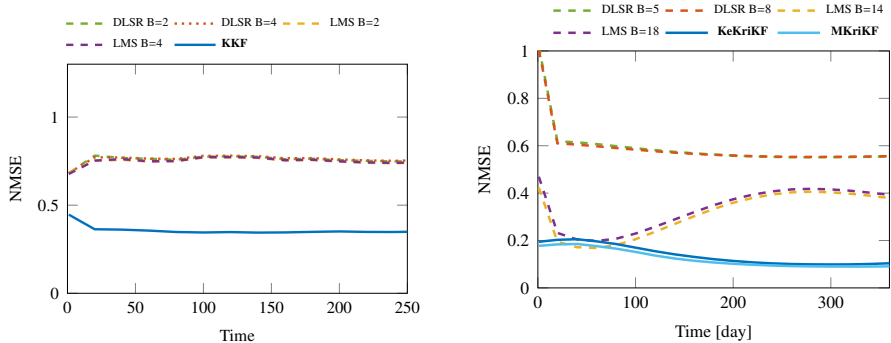
3.3 Numerical tests

This section compares the performance of the methods we discussed in §3.1 and §3.2 with state-of-the-art alternatives, and illustrates some of the trade-offs inherent to time-varying function reconstruction through real-data experiments. The source code for the simulations is available at the authors’ websites.

Unless otherwise stated, the compared estimators include distributed least squares reconstruction (DLSR) [52] with step size μ_{DLSR} and parameter β_{DLSR} ; the least mean-squares (LMS) algorithm in [53] with step size μ_{LMS} ; the bandlimited instantaneous estimator (BL-IE), which results after applying [11, 13, 15] separately per t ; and the KRR instantaneous estimator (KRR-IE) in (36) with a diffusion kernel with parameter σ . DLSR, LMS, and BL-IE also use a bandwidth parameter B .

Reconstruction via extended graphs. For our first experiment we use a dataset obtained from an epilepsy study [66], which is used to showcase an example analysis of electrocorticography (ECoG) data (analysis of ECoG data is a standard tool in diagnosing epilepsy). Our next experiment utilizes the ECoG time series in [66] from $N = 76$ electrodes implanted in a patient’s brain before and after the onset of a seizure. A symmetric time-invariant adjacency matrix \mathbf{A} was obtained using the method in [47] with ECoG data before the onset of the seizure. Function $f(v_n, t)$ comprises the electrical signal at the n -th electrode and t -th sampling instant after the onset of the seizure, for a period of $T = 250$ samples. The values of $f(v_n, t)$ were normalized by subtracting the temporal mean of each time series before the onset of the seizure. The goal of the experiment is to illustrate the reconstruction performance of KKF in capturing the complex spatio-temporal dynamics of brain signals.

Fig. 3(a) depicts the $\text{NMSE}(t, \{\mathcal{S}_\tau\}_{\tau=1}^t)$, averaged over all sets $\mathcal{S}_t = \mathcal{S}$, $\forall t$, of size $S = 53$. For the KKF, a space-time kernel was created (see [54]) with \mathbf{K}_t a time-invariant covariance kernel $\mathbf{K}_t = \hat{\boldsymbol{\Sigma}}$, where $\hat{\boldsymbol{\Sigma}}$ was set to the sample covariance matrix of the time series before the onset of the seizure, and with a time-invariant $\mathbf{B}^{(T)} = b^{(T)}\mathbf{I}$. The results clearly show the superior reconstruction performance of the KKF, which successfully exploits the statistics of the signal when available, among competing approaches, even with a small number of samples. This result suggests that the ECoG diagnosis technique could be efficiently conducted even with a smaller number of intracranial electrodes, which may have a positive impact on the patient’s experience.



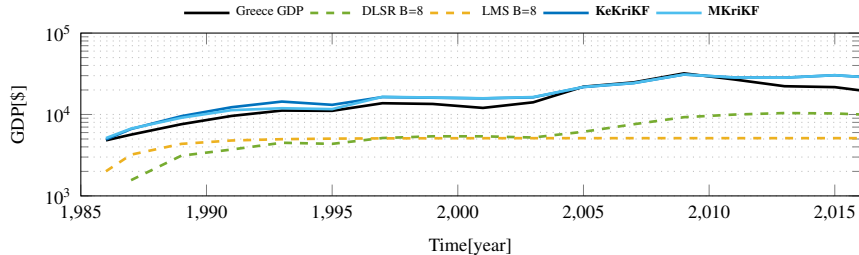
(a) NMSE for the ECoG data set ($\sigma = 1.2$, $\mu = 10^{-4}$, $\mu_{\text{DLSR}} = 1.2$, $b^{(\mathcal{T})} = 0.01$, $\beta_{\text{DLSR}} = 0.5$, $\mu_{\text{LMS}} = 0.6$). (b) NMSE of temperature estimates. ($\mu_1 = 1$, $\mu_2 = 1$, $\mu_{\text{DLSR}} = 1.6$, $\beta_{\text{DLSR}} = 0.5$, $\mu_{\text{LMS}} = 0.6$, $\alpha = 10^{-3}$, $\mu_\eta = 10^{-5}$, $r_\eta = 10^{-6}$, $\mu_\nu = 2$, $r_\nu = 0.5$, $M_\nu = 40$, $M_\eta = 40$)

Figure 3: NMSE for real data simulations.

Reconstruction via KeKriKF. The second dataset is provided by the National Climatic Data Center [67], and comprises hourly temperature measurements at $N = 109$ measuring stations across the continental United States in 2010. A time-invariant graph was constructed as in [54], based on geographical distances. The value $f(v_n, t)$ represents the temperature recorded at the n -th station and t -th day.

Fig. 3(b) reports the performance of different reconstruction algorithms in terms of NMSE, for $S = 40$. The KeKriKF Algorithm 3 adopts a diffusion kernel for $\mathbf{K}^{(\nu)}$ with $\sigma = 1.8$, and for $\mathbf{K}^{(\eta)} = s_\eta \mathbf{I}_N$ with $s_\eta = 10^{-5}$. The multi-kernel kriged Kalman filter (MKriKF) is configured with: \mathcal{D}_ν that contains M_ν diffusion kernels with parameters $\{\sigma(m)\}_{m=1}^{M_\nu}$ drawn from a Gaussian distribution with mean μ_ν and variance r_ν ; \mathcal{D}_η that contains M_η $s_\eta \mathbf{I}_N$ with parameters $\{s_\eta(m)\}_{m=1}^{M_\eta}$ drawn from a Gaussian distribution with mean μ_η and variance r_η . The specific kernel selection for KeKriKF leads to the smallest NMSE error and were selected using cross validation. Observe that MKriKF captures the spatio-temporal dynamics, successfully explores the pool of available kernels, and achieves superior performance.

The third dataset is provided by the World Bank Group [68] and comprises of the gross domestic product (GDP) per capita values for $N = 127$ countries for the years 1960-2016. A time-invariant graph was constructed using the correlation between the GDP values for the first 25 years of different countries. The graph function $f(v_n, t)$ denotes the GDP value reported at the n -th country and t -th year for $t = 1985, \dots, 2016$. The graph fourier transform of the GDP values shows that the graph frequencies f_k , $4 < k < 120$ take small values and large values otherwise. Motivated by the aforementioned observation, the KeKriKF is configured with a band-reject kernel $\mathbf{K}^{(\nu)}$ that results after applying



(a) Tracking of GDP. ($\mu_{\text{DLSR}} = 1.6$, $\beta_{\text{DLSR}} = 0.4$, $\mu_{\text{LMS}} = 1.6$, $\rho_{\nu} = 10^5$, $\rho_{\eta} = 10^5$)

Figure 4: NMSE for GDP data.

$r(\lambda_n) = \beta$ for $k \leq n \leq N - l$ and $r(\lambda_n) = 1/\beta$ otherwise in (16) with $k = 3, l = 6, \beta = 15$ and for $\mathbf{K}^{(\eta)} = s_{\eta} \mathbf{I}_N$ with $s_{\eta} = 10^{-4}$. The MKriKF adopts a \mathcal{D}_{ν} that contains band-reject kernels with $k \in [2, 4], l \in [3, 6], \beta = 15$ that result to $M_{\nu} = 12$ kernels and a \mathcal{D}_{η} that contains $\{s_{\eta}(m) \mathbf{I}_N\}_{m=1}^{40}$ with $s_{\eta}(m)$ drawn from a Gaussian distribution with mean $\mu_{\eta} = 10^{-5}$ and variance $r_{\eta} = 10^{-6}$. Next, the performance of different algorithms in tracking the GDP value is evaluated after sampling $S = 38$ countries.

Fig. 4 illustrates the actual GDP as well as GDP estimates for Greece, that is not contained in the sampled countries. Clearly, MKriKF, that learns the pertinent kernels from the data, achieves roughly the same performance of KeKriKF, that is configured manually to obtain the smallest possible NMSE.

4 Summary

The task of reconstructing functions defined on graphs arises naturally in a plethora of applications. The kernel-based approach offers a clear, principled and intuitive way for tackling this problem. In this chapter, we gave a contemporary treatment of this framework focusing on both time-invariant and time-evolving domains. The methods presented herein offer the potential of providing an expressive way to tackle interesting real-world problems. Besides illustrating the effectiveness of the discussed approaches, our tests were also chosen to showcase interesting application areas as well as reasonable modeling approaches for the interested readers to build upon. For further details about the models discussed here and their theoretical properties, the reader is referred to [23, 42, 61, 69–71] and the references therein.

Acknowledgement. The research was supported by NSF grants 1442686, 1500713, 1508993, 1509040, and 1739397.

References

- [1] E. D. Kolaczyk, *Statistical Analysis of Network Data: Methods and Models*, Springer New York, 2009.
- [2] R. I. Kondor and J. Lafferty, “Diffusion kernels on graphs and other discrete structures,” in *Proc. Int. Conf. Mach. Learn.*, Sydney, Australia, Jul. 2002, pp. 315–322.
- [3] A. J. Smola and R. I. Kondor, “Kernels and regularization on graphs,” in *Learning Theory and Kernel Machines*, pp. 144–158. Springer, 2003.
- [4] D. I. Shuman, S. K. Narang, P. Frossard, A. Ortega, and P. Vandergheynst, “The emerging field of signal processing on graphs: Extending high-dimensional data analysis to networks and other irregular domains,” *IEEE Sig. Process. Mag.*, vol. 30, no. 3, pp. 83–98, May 2013.
- [5] A. Sandryhaila and J. M. F. Moura, “Discrete signal processing on graphs,” *IEEE Trans. Sig. Process.*, vol. 61, no. 7, pp. 1644–1656, Apr. 2013.
- [6] O. Chapelle, B. Schölkopf, A. Zien, et al., *Semi-supervised Learning*, MIT press Cambridge, 2006.
- [7] O. Chapelle, V. Vapnik, and J. Weston, “Transductive inference for estimating values of functions,” in *Proc. Advances Neural Inf. Process. Syst.*, Denver, Colorado, 1999, vol. 12, pp. 421–427.
- [8] C. Cortes and M. Mohri, “On transductive regression,” in *Proc. Advances Neural Inf. Process. Syst.*, Vancouver, Canada, 2007, pp. 305–312.
- [9] M. Belkin, P. Niyogi, and V. Sindhwani, “Manifold regularization: A geometric framework for learning from labeled and unlabeled examples,” *J. Mach. Learn. Res.*, vol. 7, pp. 2399–2434, 2006.
- [10] S. K. Narang, A. Gadde, and A. Ortega, “Signal processing techniques for interpolation in graph structured data,” in *Proc. IEEE Int. Conf. Acoust., Speech, Sig. Process.*, Vancouver, Canada, 2013, IEEE, pp. 5445–5449.
- [11] S. K. Narang, A. Gadde, E. Sanou, and A. Ortega, “Localized iterative methods for interpolation in graph structured data,” in *Global Conf. Sig. Inf. Process.*, Austin, Texas, 2013, IEEE, pp. 491–494.
- [12] A. Gadde and A. Ortega, “A probabilistic interpretation of sampling theory of graph signals,” in *Proc. IEEE Int. Conf. Acoust., Speech, Sig. Process.*, Brisbane, Australia, Apr. 2015, pp. 3257–3261.
- [13] M. Tsitsvero, S. Barbarossa, and P. Di Lorenzo, “Signals on graphs: Uncertainty principle and sampling,” *IEEE Trans. Sig. Process.*, vol. 64, no. 18, pp. 4845–4860, Sep. 2016.

- [14] S. Chen, R. Varma, A. Sandryhaila, and J. Kovacevic, “Discrete signal processing on graphs: Sampling theory,” *IEEE Trans. Sig. Process.*, vol. 63, no. 24, pp. 6510–6523, Dec. 2015.
- [15] A. Anis, A. Gadde, and A. Ortega, “Efficient sampling set selection for bandlimited graph signals using graph spectral proxies,” *IEEE Trans. Sig. Process.*, vol. 64, no. 14, pp. 3775–3789, Jul. 2016.
- [16] X. Wang, P. Liu, and Y. Gu, “Local-set-based graph signal reconstruction,” *IEEE Trans. Sig. Process.*, vol. 63, no. 9, pp. 2432–2444, May 2015.
- [17] A. G. Marques, S. Segarra, G. Leus, and A. Ribeiro, “Sampling of graph signals with successive local aggregations,” *IEEE Trans. Sig. Process.*, vol. 64, no. 7, pp. 1832–1843, Apr. 2016.
- [18] B. Schölkopf and A. J. Smola, *Learning with Kernels: Support Vector Machines, Regularization, Optimization, and Beyond*, MIT Press, 2002.
- [19] B. Schölkopf, R. Herbrich, and A. J. Smola, “A generalized representer theorem,” in *Computational Learning Theory*. Springer, 2001, pp. 416–426.
- [20] V. N. Vapnik, *Statistical Learning Theory*, vol. 1, New York: Wiley, 1998.
- [21] G. Kimeldorf and G. Wahba, “Some results on Tchebycheffian spline functions,” *J. Mathematical Analysis Appl.*, vol. 33, no. 1, pp. 82–95, 1971.
- [22] D. Zhou and B. Schölkopf, “A regularization framework for learning from graph data,” in *ICML Workshop Stat. Relational Learn. Connections Other Fields*, Banff, Canada, Jul. 2004, vol. 15, pp. 67–68.
- [23] D. Romero, M. Ma, and G. B. Giannakis, “Kernel-based reconstruction of graph signals,” *IEEE Trans. Sig. Process.*, vol. 65, no. 3, pp. 764–778, 2017.
- [24] L. Page, S. Brin, R. Motwani, and T. Winograd, “The pagerank citation ranking: Bringing order to the web.,” Tech. Rep., Stanford InfoLab, 1999.
- [25] A. N. Nikolakopoulos, A. Korba, and J. D. Garofalakis, “Random surfing on multipartite graphs,” in *2016 IEEE International Conference on Big Data (Big Data)*, Dec 2016, pp. 736–745.
- [26] A. N. Nikolakopoulos and J. D. Garofalakis, “Random surfing without teleportation,” in *Algorithms, Probability, Networks, and Games*, pp. 344–357. Springer International Publishing, 2015.
- [27] J.-A. Bazerque and G. B. Giannakis, “Nonparametric basis pursuit via kernel-based learning,” *IEEE Sig. Process. Mag.*, vol. 28, no. 30, pp. 112–125, Jul. 2013.

- [28] V. Sindhwani, P. Niyogi, and M. Belkin, “Beyond the point cloud: From transductive to semi-supervised learning,” in *Proc. Int. Conf. Mach. Learn.* ACM, 2005, pp. 824–831.
- [29] M. Kivelä, A. Arenas, M. Barthelemy, J. P. Gleeson, Y. Moreno, and M. A. Porter, “Multilayer networks,” *Journal of Complex Networks*, vol. 2, no. 3, pp. 203–271, 2014.
- [30] V. N. Ioannidis, P. A. Traganitis, S. Yanning, and G. B. Giannakis, “Kernel-based semi-supervised learning over multilayer graphs,” in *Proc. IEEE Int. Workshop Sig. Process. Advances Wireless Commun.*, Kalamata, Greece, Jun. 2018.
- [31] M. Gönen and E. Alpaydm, “Multiple kernel learning algorithms,” *J. Mach. Learn. Res.*, vol. 12, no. Jul, pp. 2211–2268, 2011.
- [32] J.-A. Bazerque, G. Mateos, and G. B. Giannakis, “Group-lasso on splines for spectrum cartography,” *IEEE Trans. Sig. Process.*, vol. 59, no. 10, pp. 4648–4663, Oct. 2011.
- [33] G. B. Giannakis, Q. Ling, G. Mateos, I. D. Schizas, and H. Zhu, “Decentralized learning for wireless communications and networking,” *arXiv preprint arXiv:1503.08855*, 2016.
- [34] C. A. Micchelli and M. Pontil, “Learning the kernel function via regularization,” in *J. Mach. Learn. Res.*, 2005, pp. 1099–1125.
- [35] S. Segarra, A. G. Marques, G. Leus, and A. Ribeiro, “Reconstruction of graph signals through percolation from seeding nodes,” *IEEE Trans. Sig. Process.*, vol. 64, no. 16, pp. 4363–4378, Aug. 2016.
- [36] A. S. Zamzam, V. N. Ioannidis, and N. D. Sidiropoulos, “Coupled graph tensor factorization,” in *Proc. Asilomar Conf. Sig., Syst., Comput.*, Pacific Grove, CA, 2016, pp. 1755–1759.
- [37] A. N Nikolakopoulos and J. D Garofalakis, “Ncdawarerank: a novel ranking method that exploits the decomposable structure of the web,” in *Proceedings of the sixth ACM international conference on Web search and data mining*. ACM, 2013, pp. 143–152.
- [38] A. N. Nikolakopoulos, V. Kalantzis, E. Gallopoulos, and J. D. Garofalakis, “Factored proximity models for top-n recommendations,” in *Big Knowledge (ICBK), 2017 IEEE International Conference on*. IEEE, 2017, pp. 80–87.
- [39] A. N. Nikolakopoulos and J. D. Garofalakis, “Top-n recommendations in the presence of sparsity: An ncd-based approach,” in *Web Intelligence*. IOS Press, 2015, vol. 13, pp. 247–265.
- [40] A. N Nikolakopoulos, M. A. Kouneli, and J. D Garofalakis, “Hierarchical itemspace rank: Exploiting hierarchy to alleviate sparsity in ranking-based recommendation,” *Neurocomputing*, vol. 163, pp. 126–136, Sep. 2015.

- [41] A. N. Nikolakopoulos and J. D. Garofalakis, “Ncdrec: A decomposability inspired framework for top-n recommendation,” in *2014 IEEE/WIC/ACM International Joint Conferences on Web Intelligence (WI) and Intelligent Agent Technologies (IAT)*, Aug 2014, vol. 1, pp. 183–190.
- [42] V. N. Ioannidis, A. N. Nikolakopoulos, and G. B. Giannakis, “Semi-parametric graph kernel-based reconstruction,” in *Global Conf. Sig. Inf. Process. (to appear)*, Montreal, Canada, Nov. 2017.
- [43] V. Vapnik, *The nature of statistical learning theory*, Springer, 2013.
- [44] “Bureau of Transportation, United States,” [Online]. Available: [urlhttp://www.transtats.bts.gov/](http://www.transtats.bts.gov/), 2016.
- [45] S. Chen, R. Varma, A. Singh, and J. Kovačević, “Signal representations on graphs: Tools and applications,” arXiv preprint arXiv:1512.05406 [Online]. Available: [urlhttp://arxiv.org/abs/1512.05406](http://arxiv.org/abs/1512.05406), 2015.
- [46] U. Von Luxburg, “A tutorial on spectral clustering,” vol. 17, no. 4, pp. 395–416, Dec. 2007.
- [47] Y. Shen, B. Baingana, and G. B. Giannakis, “Nonlinear structural vector autoregressive models for inferring effective brain network connectivity,” *arXiv preprint arXiv:1610.06551*, 2016.
- [48] B. Baingana and G. B. Giannakis, “Tracking switched dynamic network topologies from information cascades,” *IEEE Trans. Sig. Process.*, vol. 65, no. 4, pp. 985–997, Feb. 2017.
- [49] F. R. Bach and M. I. Jordan, “Learning graphical models for stationary time series,” *IEEE Trans. Sig. Process.*, vol. 52, no. 8, pp. 2189–2199, 2004.
- [50] J. Mei and J. M. F. Moura, “Signal processing on graphs: Causal modeling of big data,” *arXiv preprint arXiv:1503.00173v3*, 2016.
- [51] P. A. Forero, K. Rajawat, and G. B. Giannakis, “Prediction of partially observed dynamical processes over networks via dictionary learning,” *IEEE Trans. Sig. Process.*, vol. 62, no. 13, pp. 3305–3320, Jul. 2014.
- [52] X. Wang, M. Wang, and Y. Gu, “A distributed tracking algorithm for reconstruction of graph signals,” *IEEE J. Sel. Topics Sig. Process.*, vol. 9, no. 4, pp. 728–740, 2015.
- [53] P. Di Lorenzo, S. Barbarossa, P. Banelli, and S. Sardellitti, “Adaptive least mean squares estimation of graph signals,” *IEEE Trans. Sig. Info. Process. Netw.*, vol. Early Access, 2016.
- [54] D. Romero, V. N. Ioannidis, and G. B. Giannakis, “Kernel-based reconstruction of space-time functions on dynamic graphs,” *IEEE J. Sel. Topics Sig. Process.*, vol. 11, no. 6, pp. 1–14, Sep. 2017.

- [55] G. Strang and K. Borre, *Linear algebra, geodesy, and GPS*, Siam, 1997.
- [56] I. D. Schizas, G. B. Giannakis, S. I. Roumeliotis, and A. Ribeiro, “Consensus in ad hoc wsns with noisy linkspart ii: Distributed estimation and smoothing of random signals,” *IEEE Trans. Sig. Process.*, vol. 56, no. 4, pp. 1650–1666, Apr. 2008.
- [57] T. W. Anderson, *An introduction to multivariate statistical analysis*, vol. 2, Wiley New York, 1958.
- [58] K. Rajawat, E. Dall’Anese, and G. B. Giannakis, “Dynamic network delay cartography,” *IEEE Trans. Inf. Theory*, vol. 60, no. 5, pp. 2910–2920, 2014.
- [59] C. K. Wikle and N. Cressie, “A dimension-reduced approach to space-time kalman filtering,” *Biometrika*, pp. 815–829, 1999.
- [60] Seung-Jun Kim, E. Dall’Anese, and G. B. Giannakis, “Cooperative spectrum sensing for cognitive radios using kriged Kalman filtering,” *IEEE J. Sel. Topics Sig. Process.*, vol. 5, no. 1, pp. 24–36, feb. 2011.
- [61] V. N. Ioannidis, D. Romero, and G. B. Giannakis, “Inference of spatio-temporal functions over graphs via multi-kernel kriged Kalman filtering,” *IEEE Trans. Signal Process.*, 2018 (to appear), 2017.
- [62] K. V. Mardia, C. Goodall, E. J. Redfern, and F. J. Alonso, “The kriged kalman filter,” *Test*, vol. 7, no. 2, pp. 217–282, 1998.
- [63] I. Csiszár and G. Tusnády, “Information geometry and alternating minimization procedures,” *Statistics and Decisions*, pp. 205–237, 1984.
- [64] L. Zhang, D. Romero, and G. B. Giannakis, “Fast convergent algorithms for multi-kernel regression,” in *Proc. Workshop Stat. Sig. Process.*, Palma de Mallorca, Spain, Jun. 2016.
- [65] L. Zhang, G. Wang, D. Romero, and G. B. Giannakis, “Randomized block Frank-Wolfe for convergent large-scale learning,” *IEEE Trans. Signal Process.*, 2017 (to appear); see also *arXiv:1612.08461*, 2017.
- [66] M. A. Kramer, E. D. Kolaczyk, and H. E. Kirsch, “Emergent network topology at seizure onset in humans,” *Epilepsy Res.*, vol. 79, no. 2, pp. 173–186, 2008.
- [67] “1981-2010 U.S. climate normals,” [Online]. Available: [url-https://www.ncdc.noaa.gov](https://www.ncdc.noaa.gov).
- [68] “GDP per capita (current US),” [Online]. Available: [url-https://data.worldbank.org/indicator/NY.GDP.PCAP.CD](https://data.worldbank.org/indicator/NY.GDP.PCAP.CD).
- [69] V. N. Ioannidis, D. Romero, and G. B. Giannakis, “Inference of spatiotemporal processes over graphs via kernel kriged kalman filtering,” in *Proc. European Sig. Process. Conf.*, Kos, Greece, Aug. 2017.

- [70] V. N. Ioannidis, D. Romero, and G. B. Giannakis, “Kernel-based reconstruction of space-time functions via extended graphs,” in *Proc. Asilomar Conf. Sig., Syst., Comput.*, Pacific Grove, CA, Nov. 2016, pp. 1829 – 1833.
- [71] D. Romero, M. Ma, and G. B. Giannakis, “Estimating signals over graphs via multi-kernel learning,” in *Proc. Workshop Stat. Sig. Process.*, Palma de Mallorca, Spain, Jun. 2016.